ADVANCED ENERGY MATERIALS
www.advenergymat.de

Layered Perovskites in Solar Cells: Structure, Optoelectronic Properties, and Device Design

Dumitru Sirbu, Folusho Helen Balogun,* Rebecca L. Milot,* and Pablo Docampo**

Layered hybrid perovskites (LPKs) have emerged as a viable solution to address perovskite stability concerns and enable their implementation in wide-scale energy harvesting. Yet, although more stable, the performance of devices incorporating LPKs still lags behind that of state-of-the-art, multication perovskite materials. This is typically assigned to their poor charge transport, currently caused by the choice of cations used within the organic layer. On balance, a compromise between efficiency and stability is sought, involving careful control of phase purity and distribution, interfaces and energy/charge transfer processes. Further progress is hindered by the difficulty in identifying the fundamental optoelectronic processes in these materials. Here, the high exciton binding energy of LPKs lead to the formation of multiple photoexcited species, which greatly complicate measurement interpretation. In this light, this review gives an overview of how complementary measurement techniques must be used to separate the contributions from the different species in order to identify device bottlenecks, and become a useful tool to narrow down the limitless list of organic cations. A move away from making compromises to mitigate the impact of poor charge transport is required. The root of the problem must be addressed instead through rational design of the interlayer cations.

1. Introduction

Hybrid halide perovskite absorbers have caught the imagination of researchers worldwide due to their outstanding optoelectronic properties akin to industrial juggernauts gallium arsenide and silicon.[1,2] Yet, the materials are compatible with solution-processing techniques such as inkjet printing and spray coating.[3] This unprecedented combination has led to the development of solar cells which already show power conversion efficiencies of over 25%, similar to state-of-the-art poly-Si and other thin-film technologies, in just over 10 years of development.[4]

Hybrid perovskites are particularly interesting for indoor applications, with impressive efficiencies of over 35% demonstrated under indoor illumination which may prove a viable option to power the ever expanding Internet of Things.[5] Rather than competing with the current technology giants, perovskites can work together with other solar cell technologies in a tandem configuration. Record efficiencies of over 29% for silicon-perovskite tandem solar cells have already been reported and further progress is expected in the near future.[6] Although perovskite solar cells (PSCs) are on the verge of mass production, two main challenges remain: stability[7] and toxicity.[8] Multiple reviews already address the toxicity concern, and it will not be discussed here.[9–11]

Layered hybrid perovskites (LPKs) have emerged as an answer to battle stability concerns. Although known for decades, LPKs have only recently been incorporated in photovoltaic (PV) applications, resulting in modest device power conversion efficiencies due to poorer optoelectronic properties.[12–14] However, their key advantage is the stabilizing effects of the organic interlayers, which prevents perovskite degradation.[15,16] The organic spacer inhibits ion migration which prevents the formation of irreversible degradation products.[17] Alternatively, LPKs can be deposited over the state-of-the-art perovskite materials to combine the high performance of 3D perovskites with the stabilizing properties of LPKs.[15] Here, the limiting factor is inefficient charge transport across the organic interlayer, currently preventing the full exploitation of the layered structure in PSCs.

This can be approached in two ways, either by keeping the LPK layer very thin, currently the most popular approach, or by increasing the electrical conductivity of the material.[18,19] The conductivity can be enhanced through increasing the number of inorganic layers *n*, but this comes at the price of reduced stability.[20–22] The better approach is to enhance the charge transport in LPKs through the molecular engineering of the organic

Dr. D. Sirbu
School of Mathematics, Statistics and Physics
Newcastle University
Newcastle upon Tyne NE1 7RU, UK
E-mail: dumitru.sirbu@newcastle.ac.uk
F. H. Balogun, Dr. R. L. Milot
Department of Physics
University of Warwick
Coventry CV4 7AL, UK
E-mail: helen.balogun@warwick.ac.uk; rebecca.milot@warwick.ac.uk
Dr. P. Docampo
School of Chemistry
University of Glasgow
Glasgow G12 8QQ, UK
E-mail: pablo.docampo@glasgow.ac.uk
The ORCID identification number(s) for the author(s) of this article can be found under https://doi.org/10.1002/aenm.202003877.

DOI: 10.1002/aenm.202003877

spacer, and the initial studies in this direction are discussed here.

Further progress toward highly efficient and stable PSCs incorporating LPKs is hindered by incomplete understanding of charge dynamics and transport mechanisms in these systems. Consequently, this review discusses how to accurately measure the photodynamics and charge transport in LPKs and hence identify device bottlenecks. The interplay and synergy between various measurement techniques are analyzed with the goal of obtaining a detailed spacially and time-resolved picture of the complicated charge dynamics. Finally, synthetic approaches toward LPKs with tuned optoelectronic properties will be examined, with a special focus on finding the best strategy toward improved charge transport in LPKs.

2. Layered Perovskite Structures

Since the definition of LPKs varies among researchers, it is necessary to clarify how the term is used in this review. Literature commonly refers to LPKs as 2D or quasi-2D perovskites, yet this is often confused with the macroscale geometry of the perovskite material, for example, nanoplatelets.[28,29] Herein the term LPK is used to describe the structure of the material itself, where the organic and inorganic layers alternate.

Due to the nature of the spacer cation, LPKs can form in a variety of crystal structures, the three most common being: i) The Ruddlesden–Popper (RP) phase, ii) Dion–Jacobson (DJ) phase, and iii) alternating cations in the interlayer space phase (ACI).[30] Structures formed by polymerization of RP cation monomers can be considered a separate class, PRP.[31–33] All these structures are schematically depicted in **Figure 1**.

The Ruddlesden–Popper (RP) phase (A'_2BX_4 for n = 1) is the most commonly studied and is formed by monovalent organic spacer cations (**Figure 2**a) arranged into a bilayer, with the ammonium units pointing toward the inorganic layer and binding through hydrogen bonds.[23,24] The organic bilayer is normally held together by van der Waals forces and π-π interactions in the case of aromatic spacers. A loose space between opposite facing monoammonium cations is formed in the organic bilayer, commonly referred to as van der Waals gap (Figure 1).[25,34–39] The metal halide sheets are usually laterally offset by half an octahedral unit, as depicted in Figure 1. A large distortion of the inorganic layer is commonly reported for the RP phase arising from the tilting of the metal iodide octahedra.[40,41]

The Dion–Jacobson (DJ) phase ($A'BX_4$ for n = 1) is based on diammonium cations (Figure 2b) that form hydrogen bonds on both sides with the vicinal inorganic sheets.[26,27] Linear diamine spacers cause a partial or no lateral offset of the metal halide sheets as seen in the RP phase, with the adjacent layers usually stacked on top of each other, as pictured in Figure 1. DJ perovskites typically exhibit a smaller interlayer distance and a lower structural distortion which is associated with a lower bandgap, as compared to their RP counterpart.[35] At the same time, the DJ phase is less studied due to the smaller number of readily available diamines.

The ACI phase is the least common type of layered perovskites and is based on two types of cations in the interlayer space, adopting the formula $A'A_nB_nX_{3n+1}$. Similarly to the DJ-phase, ACI perovskites show small interlayer distances and small or no lateral metal halide octahedra layer offset. In this structure, the A′-site cation is large, with most examples in the literature employing guanidinium (GA) although diammonium cations, such as, 1,4-butanediammonium are also possible.[42] The A-site is usually a smaller cation such as methylammonium (MA) or formamidinium (FA).[43–45]

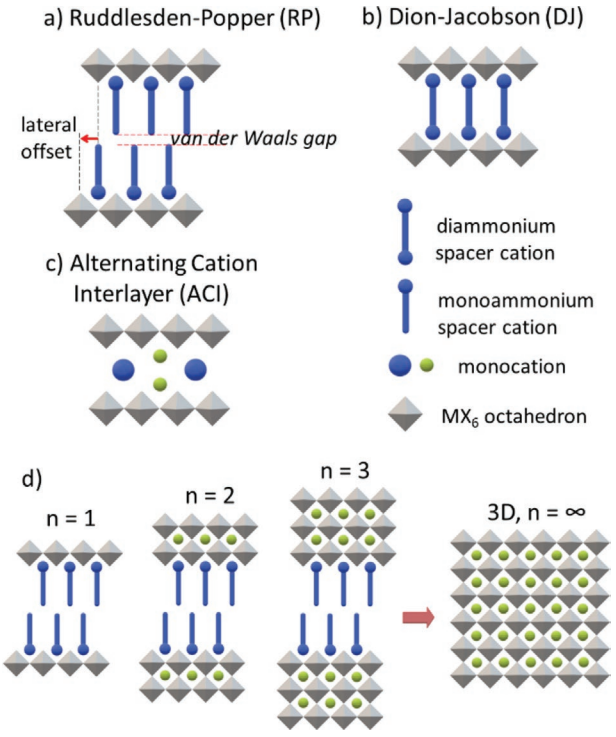

Figure 1. Schematic representation of LPK phases: a) Ruddlesden–Popper (RP) phase featuring the van der Waals gap; b) Dion–Jacobson (DJ) phase based on diammonium cations; and c) the phase with alternating cation interlayer (ACI). Note: The larger monocation in the ACI-phase can be replaced by a dication. d) Schematic representation of the RP phase LPK with increasing n = 1 to n = 3 as compared to the 3D structure.

2.1. Optoelectronic Properties of Layered Perovskites

The biggest changes to the optoelectronic properties moving from 3D perovskites to LPKs result from the differences in the exciton binding energy, which dictates the nature of the charge-carriers at the operating temperatures of devices. LPKs have large exciton binding energies up to hundreds of meV,[46,47] whereas much lower exciton binding energies have been reported for 3D structures in the range of 3 meV for low bandgap tin materials to 10s of meV for $MAPbI_3$ (MAPI).[48,49] As a result, free electrons and holes are the predominant charge-carriers in 3D materials at room temperature, although excitonic effects enhance light absorption at the band edge and may increase the efficiency of light emission.[50] Conversely, in many LPKs the majority of charge-carriers will be excitons at room temperature.[51]

These differences can be easily observed comparing the absorption and photoluminescence (PL) spectra of the two materials. Three-dimensional perovskites exhibit light absorption spectra that are characteristic of typical semiconductors with

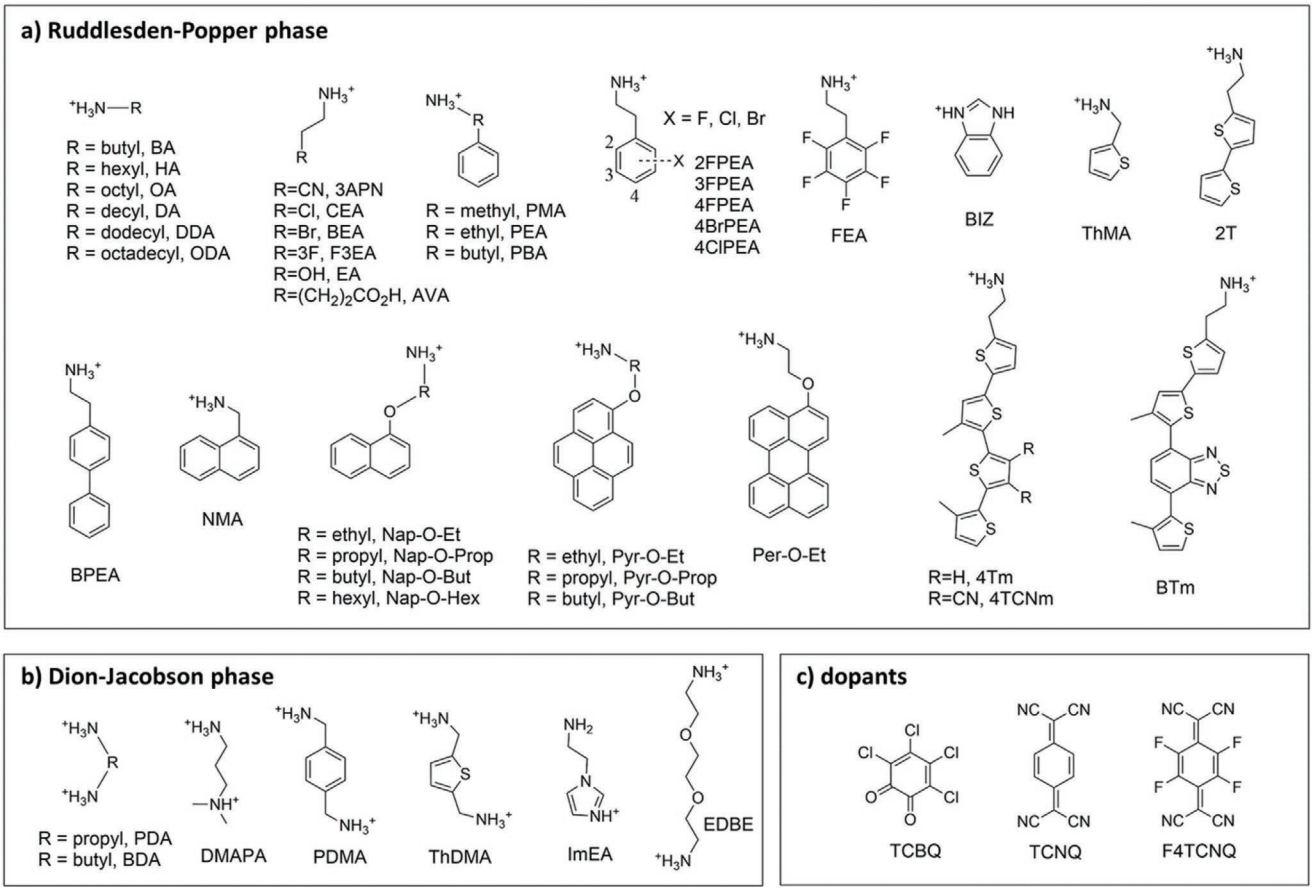

Figure 2. Collection of structures of a) RP-phase and b) DJ-phase organic spacer cations that are larger for LPK structures compared to A′-site cations in typical 3D structures. c) Structures of molecules used as dopants of the organic layer in LPKs.

primarily free charge-carriers present and are dominated by band-edge continuum absorption, as shown in **Figure 3**a.[52] In layered perovskites, an exciton transition is clearly distinguishable from the continuum due to the presence of excitonic states far below the band edge (Figure 3a,b).[52] Furthermore, the band edge for layered perovskites is blue-shifted with respect to the 3D material as a result of confinement effects, as shown in Figure 3a.

These increased exciton binding energies are a function of both decreased dimensionality of the material, imposed by the layered structure, and dielectric confinement caused by the dielectric mismatch between the metal halide and organic cation layers (Figure 3c).[51,54] There is a debate in the literature about the extent to which these excitons are localized in $n = 1$ LPKs, and it has been suggested that they are somewhere between the limits of Wannier excitons, which extend over multiple unit cells, and Frenkel excitons localized on a single unit cell.[51] In either case, the closer association of electrons and holes caused by exciton binding inhibits charge transport, which helps

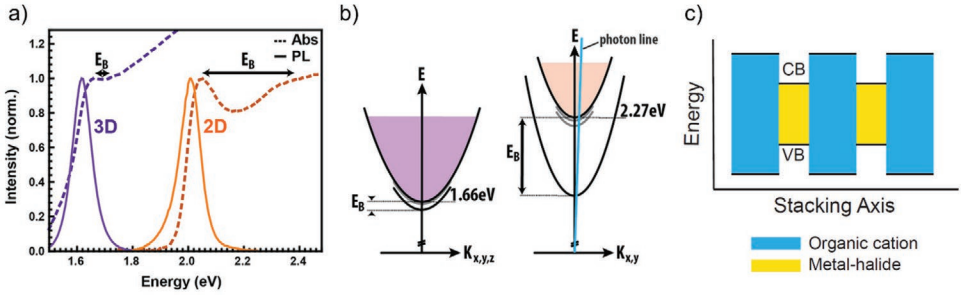

Figure 3. a) UV–vis and PL spectrum of a thin film of MAPI and an analogous $n = 1$ layered perovskite. b) Corresponding dispersion relations for the spectra, highlighting the differences in binding energies between 3D and layered perovskites. a,b) Reproduced with permission.[53] Copyright 2018, American Chemical Society. c) Schematic of the effects of dielectric and quantum confinement which give layered perovskites such high exciton binding energies.

explain why devices fabricated with $n = 1$ LPKs achieve such low efficiencies—typically less than 4%.[55,56]

2.2. Structural Tailoring of Optoelectronic Properties

One of the major advantages of using LPKs in optoelectronic devices is their high degree of tunability. Simple structural modifications of the spacer cation have a particularly strong influence on the bandgap and exciton binding energy of the resulting materials. This section details the different synthetic approaches used to optimize these properties. These include tuning the interlayer spacing, adjusting the bond angle distortion, and reducing the dielectric mismatch.

2.2.1. Interlayer Spacing

The interlayer spacing partially determines the degree of electronic coupling between the inorganic metal halide layers which has a strong effect on the bandgap and binding energy of the resulting layered material.[60,61] For example, the small DJ-spacer *p*-xylylenediamine (PDMA) was shown to lead to non-confined structures at $n > 3$ with an interlayer distance of only 3.4 Å (**Figure 4**a).[57] This results in a reduced bandgap below 1.7 eV and lowered exciton binding energy down to 69 meV corresponding to a free charge carrier to exciton ratio of 97.9% under operating photovoltaic conditions. However, at larger d-spacings above 20 Å, systematic experimental and theoretical studies on aliphatic spacers have found the bandgap (2.7 eV) and exciton binding energy (320 meV) to be mostly independent of interlayer distance.[62,63]

2.2.2. Lead Halide Bond Distortion

The bandgap and exciton binding energy of LPKs can be fine-tuned by modifying the distortion of the inorganic layer. Here, the reduction of the Pb-X-Pb angle, as shown in Figure 4b, leads to an increase in the bandgap and exciton binding energy as shown by Mitzi and many others.[19,58,59] This correlation between bond angle and perovskite optoelectronic properties has been previously studied for the 3D systems. Knutson et al. have shown that maximum metal-halide orbital overlap is achieved at angles of 180° causing a reduction in the bandgap as high as 0.3 eV in Sn-based systems.[59,64] Importantly, the change in the Pb—X—Pb bond angle between adjacent PbI_6 octahedra has a larger impact than the variation of bond angles and bond lengths within the PbI_6 octahedron.

Primary ammonium cations tend to produce stronger octahedral tilting ranging from 140° to 160° due to strong hydrogen bonding between the ammonium units and the halides.[59,65] This is reduced to above 170° for LPKs based on non-primary amines.[66,67] As a result, the octahedral tilting in LPKs was linked with changes in the bandgap from 2.29 eV for an "ideal" 180° angle to 2.42 eV for 150°. Alternatively, small modifications such as simple halogenation (2-ortho, 3-meta, 4-para) of the phenyl ring in phenylethylammonium (PEA) allow for tailoring of the

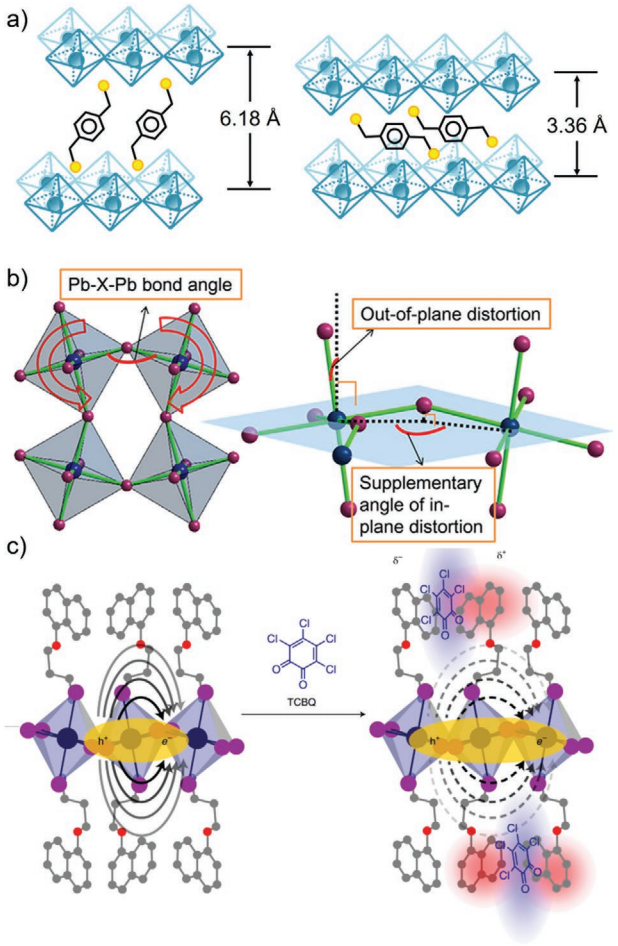

Figure 4. Examples of structural tailoring of LPK optoelectronic properties. a) Lead halide interlayer tuning. Schematic structures of confined and non-confined arrangement of the PDMA cation, the determined exciton binding energy. Reproduced with permission.[57] Copyright 2019, Wiley-VCH. b) Lead halide bond distortion. Illustration of the interaction between the ammonium unit and the halide ions inducing the distortion of the perovskite layer. Reproduced with permission.[58,59] Copyright 2017, American Chemical Society. Copyright 2005, American Chemical Society. c) Representation of the doping effect with TCBQ (blue). Doping of the pristine layer with low dielectric constant results in donor–acceptor interactions (colored in red and blue) between the electron-rich organic spacer and the electron deficient dopant molecule. Arrows represent the electron–hole coulombic interaction that is more efficiently screened by the doped organic layer thus lowering the exciton binding energy. Reproduced with permission.[47] Copyright 2020, Nature Publishing Group.

intermolecular packing and ordering in the organic layer.[68,69] The resulting reduced distortion of inorganic sheets lowers the bandgap by about 100 meV as a result of a higher valence band, along with about 40 meV reduction in exciton binding energy.[69] Additionally, introducing a competing intramolecular hydrogen bond reduces the strength of the hydrogen bond, and thus minimizes structural distortion. This can be accomplished, for example, by ether linkage in the Pyr-O-Prop spacer, as shown in Figure 4b.[19] The intramolecular cyano—ammonium H-bonding in the organic layer of $(3APN)_2PbI_4$ results in an almost "ideal" undistorted structure that reduces the bandgap to 2.2eV and lowers the valence band (VB) to −5.9 eV.[70]

2.2.3. Dielectric Constant

Increasing the dielectric constant of the organic layer (normally $\varepsilon = 3$–5 as compared to ≈30 for 3D perovskites) decreases the dielectric confinement, by reducing the dielectric mismatch in organic/inorganic layers. This, in turn, can decrease the energy required to split the exciton into free charges.[71,72] One approach to achieving this consists in the use of polar organic spacers; for example, the high dipole moment of 2,2,2-trifluoroethylammonium spacer F3EA leads to a moderate reduction of the exciton binding energy to 128 meV, from about 147 meV found for n-butylammonium (BA).[73] A dramatic 20-fold reduction in exciton binding energy was found when employing ethanolammonium (EA) when compared to the PEA analogue, as determined from temperature-dependent PL measurement.[74] This was attributed to the much higher dielectric constant of approximately 37 for the EA organic spacer compared to $\varepsilon = 3.4$ for PEA.

A different approach toward reducing the dielectric mismatch in LPKs consists of the recently emerged concept of introducing electron-acceptor molecules (Figure 2c) within the organic interlayer.[47] This can result in the formation of a donor–acceptor pair which increases the dipole moment of the organic layer, as schematically pictured in Figure 4c. This, in turn, results in a higher dielectric constant and reduces the exciton binding energy.[47,75–77] This original approach opens a new way toward tailoring the optoelectronic properties of LPKs by using commercially available small dopants and the great variety of existing organic spacers. In the pioneering work by Passarelli et al. a small organic electron-acceptor molecule, tetrachloro-1,2-benzoquinone TCBQ, was introduced to the organic layer formed by the naphthalene-based ammonium cations (Nap-O-R, R = ethylammonium, propylammonium, butylammonium, hexylammonium).[47]

2.3. $n > 1$ Layered Perovskites

So far, we have considered the "classic" LPK structure where only one layer of metal halide octahedra ($n = 1$) is sandwiched between the organic spacer layers. When more than one metal halide sheet is sandwiched between the organic spacers, a multi-n LPK structure is formed (Figure 1).[20–22] The general formula $A'_2A_{n-1}Pb_nI_{3n+1}$ corresponds to the RP phase and $A'A_{n-1}Pb_nI_{3n+1}$ for the DJ phase, where n represents the number of inorganic layers and A implies the presence of a smaller organic cation, such as, MA.

LPKs with $n > 1$ present a synthetic challenge, and it is difficult to synthesize phase pure materials.[78] An example is shown in **Figure 5**a, which shows the UV–vis and PL spectra for a nominally $n = 2$ film.[52] Multiple excitonic features and bandgap-like absorption are observed. This implies the concomitant presence of phases with different n, as the differences in thermodynamic stability become smaller at higher n values.[40] In this review, we refer to this composite material as a multi-n layered perovskite. Additionally, the PL is emitted from the red end of the absorption spectrum, which suggests charge transfer to higher n-value regions prior to emission. This hypothesis has been confirmed by several transient absorption studies[79,80] and will be discussed in more detail in Sections 4.3–4.6.

As the number of layers increases, the properties of multi-n LPKs better resemble the 3D perovskites and their "2D nature" gradually fades away, that is, the bandgap decreases, as shown in Figure 5b, the exciton binding energy becomes smaller, and they become more susceptible to degradation.[82–85] As a result, the percentage of charge-carriers existing as free carriers increases with increasing n, as shown in Figure 5c and discussed in greater detail in Section 5.1. On balance, a compromise between efficiency and stability is sought and involves careful control of phase purity and distribution, interfaces and energy/charge transfer processes.[85–87]

3. Stability of Perovskite Materials

Perovskite stability still remains the Achilles heel of the technology, primarily affected by moisture, oxygen, UV light, thermal stress, and ion migration. A concerted worldwide effort has resulted in great progress with devices showing <5% power conversion efficiency (PCE) loss for several months, including tandem configurations,[88] however, this is far from the 25 year lifetime guarantee

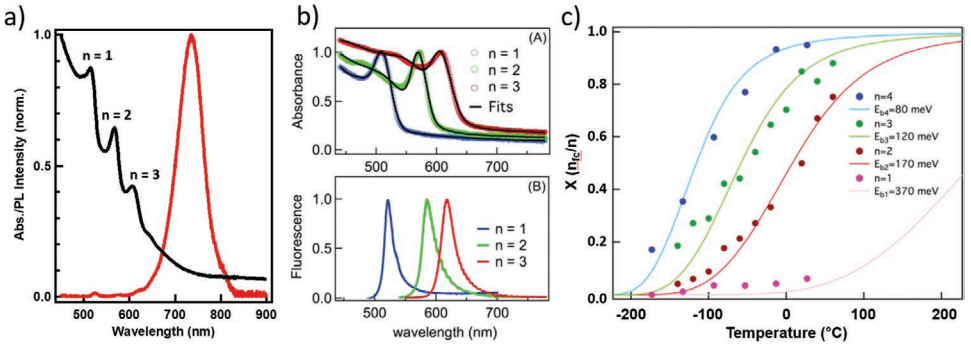

Figure 5. a) UV–vis and PL spectra of a nominally $n = 2$ thin film of $(PEA)_2MA(PbI_2)_2$. The presence of multiple excitonic peaks indicates that the film is a mixture of materials with a range of n values. Reproduced with permission.[81] Copyright 2016, American Chemical Society. b) UV–vis (top) and PL spectra for $(BA)_2(MA)_{n-1}(PbI_2)_n$ crystals with $n = 1$, 2, and 3. Reproduced with permission.[82] Copyright 2015, American Chemical Society. c) Fraction of free charges as a function of temperature for $(BA)_2(MA)_{n-1}(PbI_2)_n$ crystal estimated from time-resolved microwave conductivity measurements (dots) and modeled with the Saha equation (lines). Reproduced with permission.[83] Copyright 2017, American Chemical Society.

industry requires for PV modules.[89] While better encapsulation techniques can partially address some of these degradation pathways, thermal- and ion migration-induced degradation must be addressed at the materials design level. In this context, LPKs have made major inroads as the organic spacer layer can be tailored to address these issues. For additional information on general perovskite stability, we refer readers to other reviews focused on the stability concerns of perovskite materials.[7,90,91]

3.1. State-of-the-Art Perovskite Degradation

Thermal stress in typical hybrid halide perovskites induces a release of I_2 which leads to the appearance of metallic Pb even in the dark, leading to device performance losses.[7,92] Thermal instability can be minimized through the partial or complete substitution of MA, as well as, iodide in the structure.[93–95] Alternatively, Wang et al. have shown that redox shuttles, such as Eu^{3+}-Eu^{2+}, can reverse the formation of Pb^0 and $I_2{}^0$ through reoxidation to Pb^{2+} and reduction to I^- simultaneously in a cyclic process.[96]

Water interacts strongly with hybrid lead halide perovskites. Under very humid environments or when water condensation occurs on the surface, irreversible degradation products are formed; that is, HI (soluble in water), solid PbI_2, and CH_3NH_2 either released as gas or dissolved in water.[97] When the films are exposed to cool humid air, water is incorporated into the crystal to form a reversible mono-hydrated phase followed by a di-hydrated crystal phase.[98] In this case, the structure can be recovered by simple drying under a nitrogen stream.[98]

Here, depending on the stoichiometry used, that is, a small 5–10 mol% MA or lead excess, the resulting films exhibit different degradation products and rates. Petrus et al. showed that a small PbI_2 excess in the films improved the stability of the perovskite compared to stoichiometric samples.[99] This excess PbI_2 formed a "protective" layer at the perovskite grain boundaries, effectively terminating the perovskite crystals with Pb and I which has been calculated to be more resistant to water ingress.[100,101] On the other hand, the presence of humidity during film processing can significantly influence the thin film morphology and can be used to improve solar cell performance.[99,102] For example, exposure to moisture of MAI-excess films, followed by dehydration (so-called solvent annealing), leads to recrystallization to larger, highly oriented crystals with fewer electronic defects and a remarkable improvement in photocurrent.[99]

The effects of ion migration on device and structural stability is considerably more complex to identify and mitigate. Here, defect formation during the fabrication of perovskite films leads to unoccupied organic cation and halide lattice sites. This results in the formation of an ion with the opposite charge as the missing species, for instance a halide vacancy results in a positive ion, much like how a hole is the absence of an electron. These ions are mobile with activation energies in the region of 0.1–0.6 eV, matching values achieved for advanced superionic conductors.[103–106] Ion diffusion is heavily influenced by environmental variables and increases at higher temperatures, under an external bias or under sunlight illumination.[107,108] The existence of mobile ions in the film is undesirable for PV applications as it results in "anomalous" hysteresis, and hence unreliable device performance.[109] This has spurred hundreds of researchers to eliminate ion migration from the structure.

In this context, ion migration has been linked to a number of structural and device degradation processes including corrosion of metal contacts, halide segregation, and amorphization of the perovskite structure.[110–112] Grain boundaries in perovskite films are believed to facilitate ion migration and thus initiate the degradation process through the accumulation of ions at the interfaces.[110,113] Ion-induced degradation can be mitigated to a large extent by passivation of the grain boundaries, for instance by employing ionic liquids, which results in greatly reduced ion migration and improved stability.[114]

3.2. Enhancing Stability with Layered Structures

The superior stability of the layered perovskite structure is the main drive for their substitution or incorporation into the prototypical 3D perovskite materials. Until recently, the established thinking was that the hydrophobic nature of the bulky organic spacers was responsible for the enhanced moisture stability of LPKs.[115,116] Certainly, the layered materials are more stable in high humidity conditions. This is mainly attributed to the large cations forming a protecting layer against water ingression into the structure, thus preventing the chain of reactions ultimately leading to the irreversible formation of PbI_2.[115,117,118] However, this postulation has been put under question by a number of recent studies.

Schlipf et al. directly probed whether layered perovskites can indeed act as a water barrier in a detailed in-situ grazing-incidence small-angle neutron diffraction experiment. They compared "bare" MAPI and a second sample incorporating a PEAMAPI/MAPI heterojunction,[17] that is, using an LPK to protect the underlying 3D perovskite. Their results show that on both samples, water is first adsorbed on the surface at <35% humidity content,[17] resulting in rapid "recrystallization" of the layered perovskite material from a single $n = 5$ system to a mixture of $n = 2$ and $n = 3$ layered perovskites and MAPI, as shown in **Figure 6**a. However, after this threshold, the water starts infiltrating into the 3D perovskite for both samples, forming the hydrated phase. This clearly shows that the layered perovskite does not present a barrier against moisture ingress. Critically, the study highlights that the LPK blocks the escape of MAI, making the degradation process reversible, further affirming that LPKs suppress both vacancy migration, as well as, interfacial ion migration.[119–121]

In devices, the introduction of an LPK layer between the 3D material and the hole transporting material (HTM) has been shown to improve device stability and reduce hysteresis.[115,123–125] For instance, Grancini et al. showed that the aminovaleric acid (AVA) based perovskite ($(AVA)_2PbI_4/CH_3NH_3PbI_3$) is stable for one year. They additionally showed 10 × 10 modules with 11.2% efficiency with no loss in performance for >10 000 h under controlled standard conditions (short circuit under 1 sun illumination).[89,126] The approach also works in combination with inorganic HTMs, as shown by Chen et al. who showed that in combination with CuSCN, un-encapsulated device stability significantly improved while simultaneously reducing hysteresis.[124]

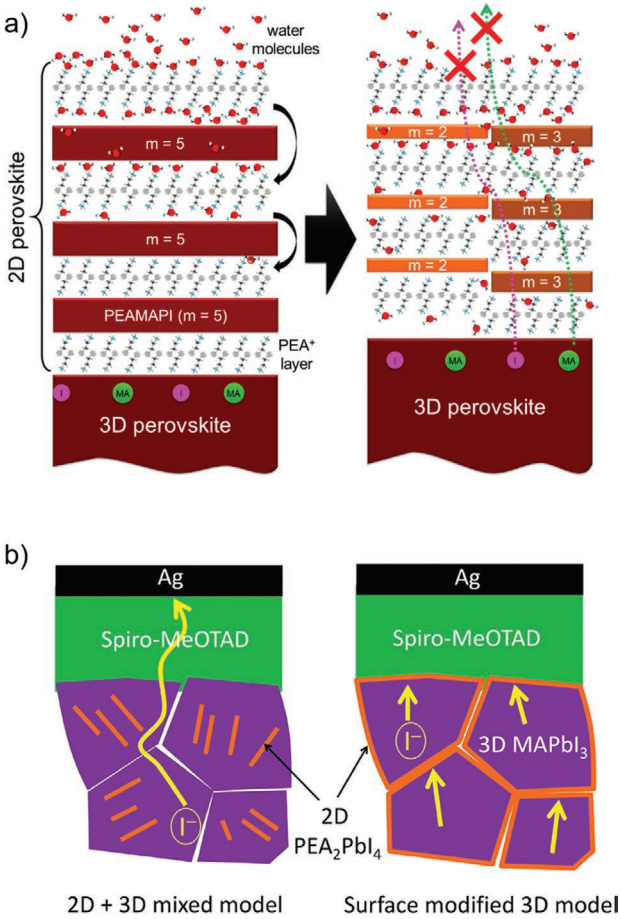

Figure 6. Schematic representation of processes related to the stability of LPKs. a) Graphic model of 3D perovskite covered with LPK illustrating the ingression of water and suppression of water-induced MAI loss that stops the irreversible material degradation. Reproduced with permission.[17] Copyright 2019, American Chemical Society. b) Illustration showing the iodide migration in 3D perovskite with dispersed LPK "platelets" and the inhibition of this migration by 3D perovskite surface passivation with LPK. Reproduced with permission.[122] Copyright 2017, American Chemical Society.

Further evidence that suppressing ion migration is a winning strategy to minimize device degradation is given by Chen et al.[122] The authors introduced ultrathin LPKs at the grain boundaries of standard 3D perovskites, resembling "bricks and mortar" as depicted in Figure 6b. This resulted in significant stability gains, as compared to a standard MAPI-based device with the improvements ascribed to the increase in activation energy for ion migration. Zhang et al.[127] also showed stability improvements in single crystal photodetectors when switching to an LPK with a measured 0.88 eV activation energy for ion migration, significantly higher than the 0.1–0.6 eV reported for MAPI.[128]

The cation design rules that maximize the suppression of ion migration are not clear at this time. However, some hints are given by experiments incorporating "rigidified" organic interlayers. For instance, fluorination of the layered cations leads to stronger intermolecular interactions, and this has been shown to improve the stability of devices by multiple reports.[68,69,129,130] Linking this to ion migration, Shi et al. reported a drastic reduction of the in-plane ion interdiffusion at I-Br interfaces employing rigid π-conjugated cations.[131] They compared a thiophene-derived cation versus a BA-based analogue and showed a reduction of three orders of magnitude in in-plane ion interdiffusion. In fact, the increased order and rigidity of organic spacers at the interface allowed the growth of near-atomically sharp epitaxial multiheterostructures with stable interfaces. However, the mobility of halide ions increases with the larger number of inorganic layers n in multi-n perovskite systems, as they gain more "3D character." Kamat and coworkers tracked the changes in the absorption spectra at the iodide/bromide heterojunction to show that the thermal activation energy of halide exchange decreases from 72 kJ mol^{-1} (n = 1) to 58 kJ mol^{-1} (n = 10), as compared to 51 kJ mol^{-1} reported for MAPI.[132,133]

3.3. Phase Stability of Dion–Jacobson Perovskites

The vast majority of studies on the stability of LPKs has been performed on the RP-phase, leaving a clear gap in our understanding. Yet, materials that form the DJ phase are worth exploring, as they avoid the van der Waals gap in the organic sheet, which is expected to lead to a more robust 2D structure.[25] Indeed, the weak van der Waals interaction in the organic bilayer in the RP phase is seen by many authors as a weak point in the structure.[25,34] In fact, this has been successfully exploited for exfoliation to form ultra-thin layers of LPKs, opening new application avenues.[134–136]

DJ perovskite phases are expected to be more rigid than RP phase counterparts. Indeed, temperature-induced structural fluctuations are suppressed in DJ LPKs.[35] Theoretical work by Ghosh et al. shows that the lack of the van der Waals gap and short interlayer distances allow for non-covalent halogen interactions between the inorganic layers. This leads to significantly reduced fluctuations compared to the model systems incorporating standard n-butylammonium (BA) and PEA cations. Shang and coworkers predict higher binding energy for the DJ perovskites, up to 7.7 eV, as compared to the RP phase, 4.0 eV for the standard PEA cation.[137] This suggests additional resistance of DJ-materials against degradation, as the monocationic spacers are much easier to dissociate from the structure.

The higher stability of the DJ materials translates into significantly longer lifetimes reported for DJ-phase PSCs, as compared to the RP counterparts.[25,138,139] Specifically, the more rigid and robust DJ structure has been shown to provide improved stability of devices toward humidity, heat, and light.[139–142] For example, replacing the pentylammonium PA cation with 1,3-propanediammonium DJ-spacer in (PDA)$(MA)_3Pb_4I_{13}$ results in remarkable stability enhancement toward humidity.[25] Here, devices retain 95% of the initial PCE after continuous aging for 168 h under 85 °C and RH 85% conditions; devices under standard light soaking conditions, retain 95% of the initial PCE for 3000 h. Furthermore, partial or full substitution of the MA-cation with the more thermally stable FA can lead to stability improvements.[143,144] For instance, a 2.5 times higher decomposition activation energy (E_a = 184.7 kJ mol^{-1}) was reported for (PDA)$(FA)_3Pb_4I_{13}$ resulting in 86% PCE retained for 1000 h at 85 °C, whilst the (PDA)$(MA)_3Pb_4I_{13}$ analogue with E_a = 74.3 kJ mol^{-1} degrades to 50% of the original PCE in only 100 h.[145] Finally, DJ-spacers can be used to

increase the stability of structures that do not incorporate lead. For example, 1,4-butanediamine was shown to stabilize the $FASnI_3$ perovskite in ambient atmosphere at RH 40%.[138]

Similarly to monodentate cations used in the RP phase, the trend of increasing cation "rigidity" leading to higher stability holds. For example, rigid cyclic structures have been shown to provide increased stability compared to linear alkyl chains. Indeed, solar cells built with trans-1,4-cyclohexanediamine retained 95% PCE after >1000 h of storage in 50–60% humidity.[139] In the same study, solar cells incorporating a linear alkyl chain—1,6-diaminohexane—dropped to 41% of initial PCE in less than 200 h.

4. Measuring Optoelectronic Properties of Layered Perovskites

In the previous sections we have briefly covered the basic electronics and stability in hybrid metal halide perovskite materials. Although great progress in device efficiencies has been achieved, current efforts are hindered by a lack of understanding of the fundamental optoelectronic processes in layered perovskites. This is a challenge due to multiple overlapping features that require complementary measurements to fully resolve. Therefore, in this section we cover how appropriate measurements can be made and interpreted in this context.[51,146,147]

4.1. Time-Resolved Pump/Probe Techniques

The appeal of time-resolved techniques for studying optoelectronic properties is their ability to unlock valuable information about charge carrier dynamics and transport occurring at timescales typically ranging from femtoseconds to milliseconds. Here, the options available for both pump and probe wavelengths from X-ray to microwave frequencies enable the study of a range of phenomena including exciton-polaron interactions, phonon modes and exciton formation. However, the specificity in the choice of pump and probe wavelengths means that no one technique is capable of fully characterizing all these processes simultaneously. **Table 1** summarizes the main techniques available, detailing the spectral features that they probe and the main limitations that they have. Transient absorption, terahertz (THz), PL, and microwave spectroscopies will be discussed in more detail below since they are the techniques that have been most used to study LPKs.

4.2. Transient Absorption Spectroscopy

Investigating the transient UV–visible absorption spectrum allows for the study of charge-carrier dynamics and excitonic effects of the material at picosecond to nanosecond timescale ranges. This is especially important for layered perovskites as excitonic effects are more prominent compared to 3D hybrid metal halide perovskites. To achieve this, the sample is photoexcited using a visible pump pulse, and the probe is a low intensity, broadband, white light pulse as shown in Figure 8a. With this setup, the difference in absorption (ΔA) between the absorption of the sample in the excited state and the absorption of the sample at equilibrium is determined as a function of the time delay between the pump and probe pulses.

Generally, there are four main processes that contribute to the ΔA signal. These are ground state bleach and stimulated emission, which result in a negative ΔA signal, and excited-state absorption and product absorption, which give a positive ΔA.[148] Having both positive and negative features is a benefit to TA because it facilitates the distinction of these properties as

Table 1. General overview of time-resolved measurements.

Technique	Pump/Probe	Time resolution	What is measured?	Limitations
Transient Absorption	Pump: Visible Probe: White light continuum	ps-ns	Transient UV–visible absorption spectrum Charge-carrier dynamics Excitonic effects	Many overlapping features can complicate data analysis
THz-TDS	Pump: N/A Probe: Broadband THz	ps-ns	Dark conductivity spectrum Phonon modes Refractive index	Data acquisition times can be long depending on the system
OPTP	Pump: Visible Probe: Broadband THz	ps-ns	Photoconductivity Charge-carrier dynamics Charge-carrier mobility	Detects only mobile charge carriers and excitons with small E_b Photoconductivity spectrum overlaps with phonon modes
TRIR	Pump: Visible Probe: Infrared	ps-ns	Vibrational modes, typically of organic cations	Limited in the fact that it only looks at lattice vibrations
PL	Pump: Visible Probe: N/A, emission is measured.	ps-ms	Charge-carrier dynamics Charge-carrier diffusion PL Quantum yield	See signal only from emissive states
Microwave conductivity	Pump: Visible Probe: Microwave	ns-ms	Photoconductivity Charge-carrier dynamics	Detects only mobile charge carriers Slower time resolution
X-ray spectroscopy	Pump: Visible Probe: X-ray	sub-ps	Structural information and dynamics	Facilities currently limited

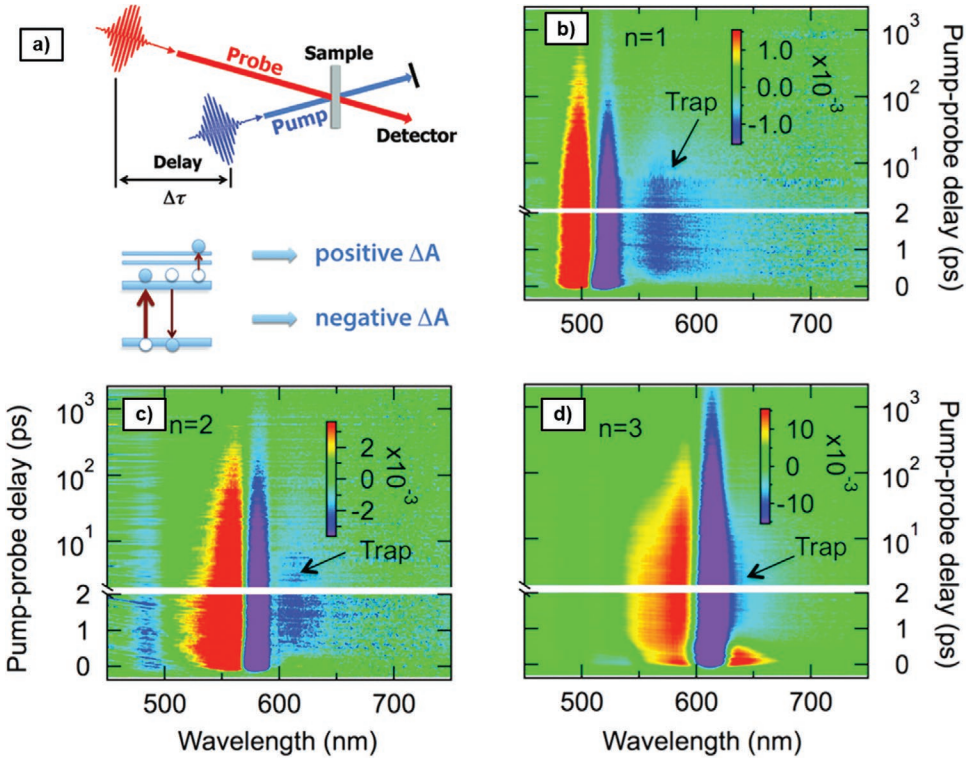

Figure 7. a) Schematic image of the transient absorption set up with the pump exciting the sample and the probe monitoring the sample's response at different times (top) and schematic of the contributions to the Δ*A* spectrum with a negative Δ*A* signal from the ground-state bleach and stimulated emission and a positive Δ*A* signal originating from excited-state absorption. Reproduced with permission.[149] Copyright 2019, de Gruyter. b–d) Psuedocolor ($-\Delta T/T_0$) TA spectra of probe wavelength versus pump-probe delay (Δt) for the layered perovskite thin film $(C_4H_9NH_3I)_2(CH_3NH_3I)_{n-1}(PbI_2)_n$: b) $n = 1$; c) $n = 2$; d) $n = 3$. Reproduced with permission.[150] Copyright 2015, American Chemical Society.

shown in **Figure 7**b–d. For a more detailed technical review of TA, see ref. [148].

Transient absorption measurements are easiest to interpret when spectral features are clearly separable. For example, Wu et al. used transient absorption (TA) to investigate exciton-exciton interactions in the layered perovskite $(BA)_2(MA)_{n-1}Pb_nI_{3n+1}$ with $n = 1$, 2, and 3.[82] They saw a distinct broadband feature below the bandgap in TA experiments as shown in **Figure 8**b–d, which they attributed to excitonic trap states and found that the density of these trap states increases with greater confinement. This is important because charge carrier trapping can be very detrimental to solar cell performance, which is covered in more detail in Section 5.1.

Analysis of features near the bandgap is more complicated because the continuum and exciton absorption overlap. In addition, absorption peaks can shift or broaden following photoexcitation, resulting in complex spectral features with both positive and negative components.[151] Accordingly for $n = 1$ materials, similar experimental data has been attributed to a range of processes including exciton thermalization, exciton-exciton annihilation, exciton trapping, polaron formation, and exciton diffusion without much consensus of the main underlying physical principles.[82,151–154]

However, many studies observe oscillations in the time-dependent TA data for LPKs that provide information about coupling between phonons and charge-carriers.[154–157] Understanding electron- or exciton-phonon coupling is essential because these interactions can place an upper limit on charge-carrier mobility and affect emission line shape. For example, Ni et al. analyzed BA_2PbI_4 and HA_2PbI_4[153] by Fourier transforming the time-domain TA signal to probe this relationship. They found that the excited-state phonon modes in BA_2PbI_4 excitons are coupled with a vibrational mode at 100 cm^{-1}, while excitons in HA_2PbI_4 are coupled to modes at 88 and 137 cm^{-1}.[153]

4.3. Terahertz Spectroscopy

In the context of PSCs, terahertz spectroscopy is primarily used to probe the mobility and carrier density of charged species, such as, electrons and holes in the picosecond timescale. Additionally, species such as low energy phonon modes, excitons, and polarons can display distinct signatures at THz frequencies (0.1–10 THz).[158,159] There are two types of ultrafast terahertz measurements commonly used to characterize materials: THz-time domain spectroscopy (THz-TDS) and optical pump/terahertz probe (OPTP) spectroscopy.

THz-TDS is analogous to steady-state transmission measurements in the far infrared. For metal halide perovskites, these spectra are typically dominated by low energy phonon modes associated with metal halide vibrational motion. These modes are important to the optoelectronic properties because they are responsible for electron-phonon scattering processes which

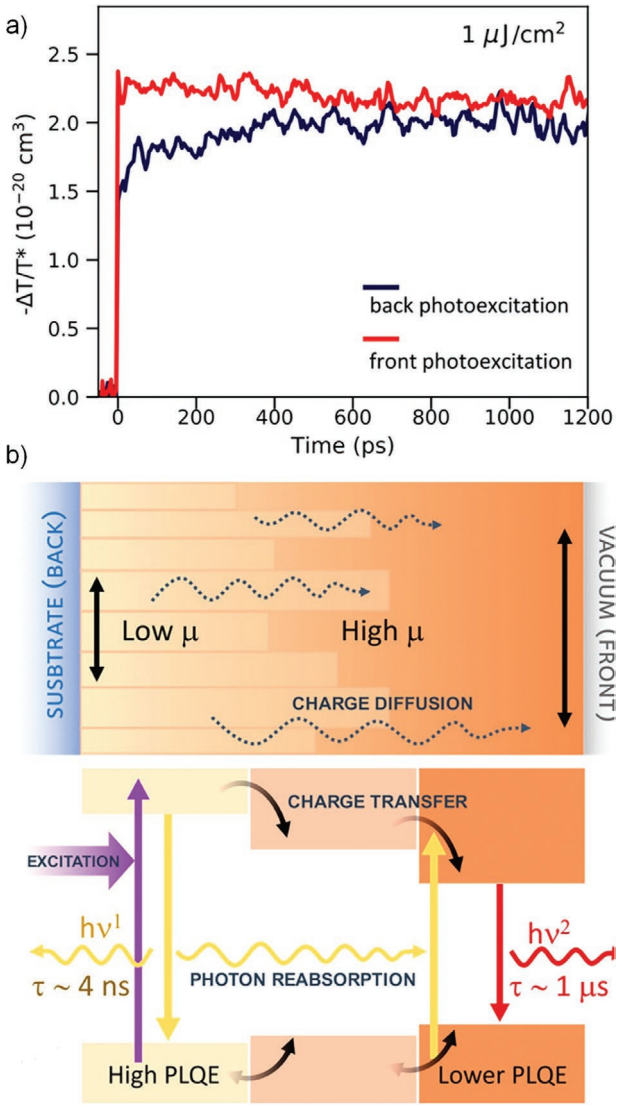

Figure 8. a) OPTP dynamics measured with illumination incident on the front (red) or back (dark blue) side of the thin film, with fluence 1 μJ cm^{-2}. b) Schematic diagram of the charge-carrier transfer and recombination mechanism involved in a thin metal halide perovskite film made of LPK, higher bandgap domains near the substrate side, and a 3D, lower bandgap region near the front (vacuum) side. Reproduced with permission.[166] Copyright 2019, American Chemical Society.

affect the mobility of the material.[160] Due to the polar nature of these materials, charge carriers interact strongly with longitudinal optical (LO) phonon modes via the Frölich mechanism.[161] Since the LO phonon frequencies are low in hybrid perovskite systems compared to other semiconductors such as GaAs, this scattering mechanism dominates at room temperature, limiting charge mobility. Although there has been work exploring the vibrational modes of 3D perovskites using THz spectroscopy,[162–164] this is a relatively unexplored area in LPKs. Such studies would therefore be a good area for further development, for example, in investigating the potential for spacer cations to influence these LO phonon modes.[165]

OPTP is a time-resolved technique where the terahertz pulse acts as the probe, and an optical pulse serves as the pump. As with transient absorption spectroscopy, changes in the absorption of THz radiation can be mapped over time (Figure 8a). Here, the change in THz transmittance $\Delta T/T$ as a function of pump/probe delay time is directly proportional to the change in photoconductivity $\Delta\sigma(\omega)$. Furthermore, the measured photoconductivity is equal to the product of the charge-carrier density n, charge-carrier mobility μ, and photon-to-charge branching ratio φ. This allows the determination of mobility in addition to measurements of charge-carrier dynamics and as a result has been extensively used to study a range of 3D perovskite materials.[162,167–171]

An important note for OPTP measurements in layered perovskites is the value of φ. In 3D perovskites, where excitonic effects are small, φ is usually equal to 1 since all the absorbed photons from the pump pulse led to the creation of mobile charges. In layered perovskites, the presence of excitons reduces φ, meaning that OPTP measurements provide only effective charge-carrier mobilities because they only take into consideration the free charge carriers and not excitonic carriers. This property is highlighted in the work by Milot et al., where increasing the n value results in a decrease in the measured charge-carrier mobility. Similarly, measurements of carrier dynamics are more representative of free charge carriers than excitons.

Far from being a disadvantage, however, this property can allow for the measurement of the timescale of charge transfer between regions with different mobilities which can be difficult with other techniques including transient absorption and PL. This usefulness is demonstrated in a study by Motti et al. on a bilayer film of an LPK and a 3D material as shown in **Figure 9**a. They found that the LPK side of the film has an initial effective charge-carrier mobility of 17.4 ± 0.9 cm^2 V^{-1} s^{-1}, where this value is increased to 23.9 ± 0.9 cm^2 V^{-1} s^{-1} for the 3D side. Their results show transfer of charge-carriers from the LPK region to the 3D region as an increase in the photoconductivity over a timescale of 1 ns. As this charge migration is so fast, it can outcompete recombination processes within the LPK region, opening implementation avenues for LPKs in devices as shown in Figure 8b.[166]

4.4. Time-Resolved Microwave Conductivity Spectroscopy

Microwave radiation, similarly to THz, interacts with mobile charge carriers in proportion to the carrier density and mobility. This allows for the determination of charge-carrier mobility in addition to charge-carrier dynamics. However, the need to place the sample in a cavity to enhance the sensitivity of the measurement limits the time resolution to ≈10–60 ns.[172,173] In time-resolved microwave conductivity (TRMC) spectroscopy, mobile charge carriers are generated in a sample using either an optical excitation pulse or a short pulse of high energy electrons. Then, a microwave pulse is sent through the material, and the transmittance of the microwave pulse is analyzed as a function of time as shown in Figure 9a.

As LPKs can exhibit charge-carrier lifetimes on the order of 50 ps or less,[175] the dynamics in many materials would be too fast for microwave conductivity to measure, and TRMC should thus be used on layered perovskites with caution. However, TRMC is suitable for materials with more 3D character and its associated longer lifetimes. For example, Gao et al. investigated the effect of using the triple cation layered perovskite thin film $BA_2(Cs_{0.02}MA_{0.64}FA_{0.34})_4Pb_5I_{16}$ compared to its monocation counterpart $BA_2(Cs_{0.02}MA_{0.64}FA_{0.34})_4Pb_5I_{16}$

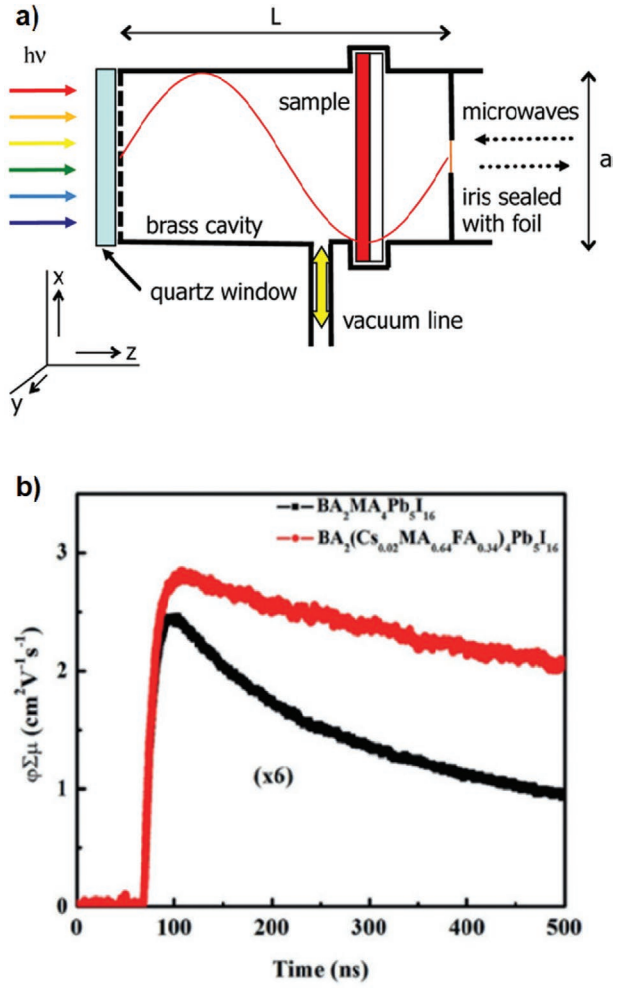

Figure 9. a) Schematic diagram of the microwave cavity to determine the change in conductance. Reproduced with permission.[173] Copyright 2013, American Chemical Society. b) Time-resolved microwave conductivity decays of $BA_2(Cs_{0.02}MA_{0.64}FA_{0.34})_4Pb_5I_{16}$ versus $BA_2(Cs_{0.02}MA_{0.64}FA_{0.34})_4Pb_5I_{16}$ thin films on glass substrates. The higher mobility of $BA_2(Cs_{0.02}MA_{0.64}FA_{0.34})_4Pb_5I_{16}$ is evidenced by its greater change in transmission following photoexcitation. Reproduced with permission.[174] Copyright 2019, Wiley-VCH.

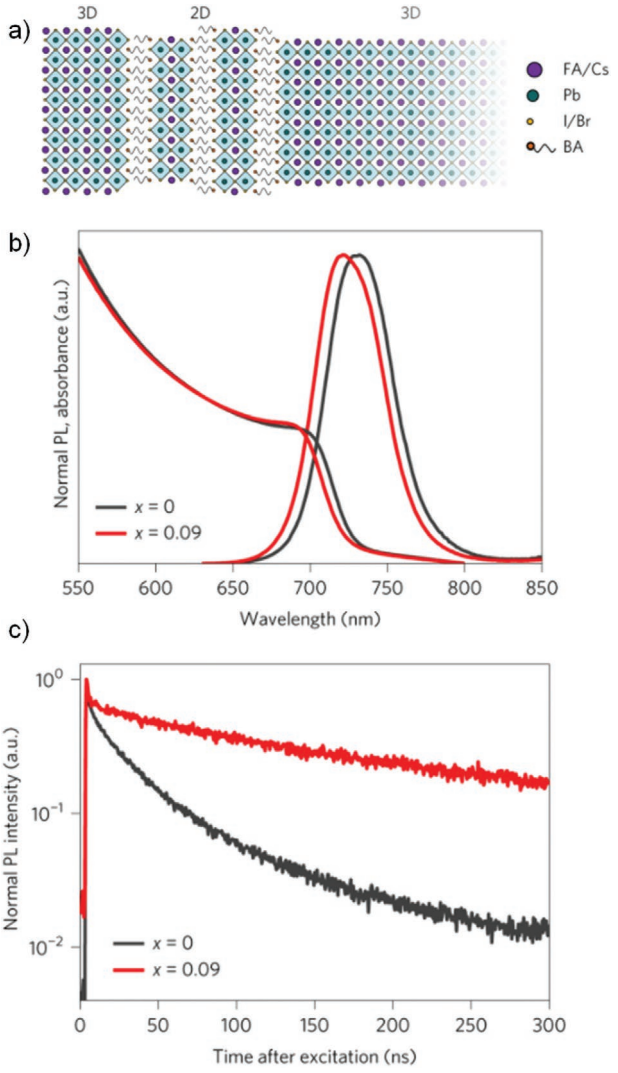

Figure 10. a) Schematic diagram of the self-assembled LPK-3D perovskite film structure. b) UV–vis and PL spectrum of an $FA_{0.83}Cs_{0.17}Pb(I_{0.6}Br_{0.4})_3$ ($x = 0$) and $BA_{0.09}(FA_{0.83}Cs_{0.17})_{0.91}Pb(I_{0.6}Br_{0.4})_3$ ($x = 0.09$) film and an $x = 0.9$ film. c) Time-resolved PL spectra for the same films. Reproduced with permission.[14] Copyright 2017, Nature Publishing Group.

using TRMC shown in Figure 9b.[174] Exciting the samples at 640 nm, they found that the effective mobility $\varphi\Sigma\mu$ was higher in $BA_2(Cs_{0.02}MA_{0.64}FA_{0.34})_4Pb_5I_{16}$ than $BA_2MA_4Pb_5I_{16}$ (2.8 $cm^2\ V^{-1}\ s^{-1}$ vs 0.41 $cm^2\ V^{-1}\ s^{-1}$). This improvement in charge transport is supported with a reduced dark carrier density for $BA_2(Cs_{0.02}MA_{0.64}FA_{0.34})_4Pb_5I_{16}$ compared to $BA_2MA_4Pb_5I_{16}$ ($n_d = 1.94 \times 10^{17}$ cm^{-3} vs $n_d = 2.58 \times 10^{18}$ cm^{-3}) which was measured using dark microwave conductivity. When combined with PL measurements, the data were able to collectively show that changing the ratios of the cations the perovskite films led to higher charge-carrier mobility, lower non-radiative recombination rates, longer charge carrier lifetimes, and faster charge transport.

4.5. Time-Resolved Photoluminescence Spectroscopy

TRPL is one of the more accessible and comparatively low cost, time-resolved techniques and is thus the one used most prevalently in the literature, making it useful for benchmarking. Additionally, TRPL is a versatile technique that can be used to obtain a large amount of information on the material's optoelectronic properties, including quantum yield and charge- carrier lifetimes, which can then be used to make conclusions about the density of trap states and the overall the quality of the film.[176] Although not technically a pump/probe technique, PL spectroscopy should be mentioned amongst these techniques due to its ability to measure many of the same dynamic processes from picosecond to millisecond timescales.

As many excitation sources for PL have low fluences, PL is most often used to provide information about monomolecular recombination processes, typically trap-mediated charge carrier recombination. This is particularly relevant to device implementation as it is critical to minimize recombination sites in order to maximize performance. For example, Wang et al. used PL spectroscopy to investigate the effect of incorporating BA cations into the 3D perovskite $FA_{0.83}Cs_{0.17}Pb(I_yBr_{1-y})_3$ shown in **Figure 10**a–c.

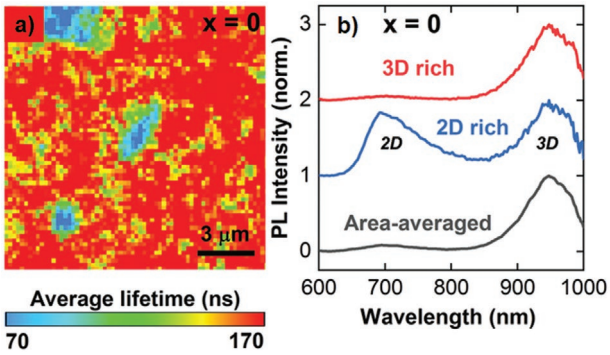

Figure 11. a) PL lifetime image of a $PEA_2FA_2(Pb_{0.5}Sn_{0.5})_3I_{10}$ thin film. The regions with a higher PEA content have associated lower lifetimes, as indicated by the blue color scaling. b) Full PL spectra from selected areas of the film in addition to an area-averaged spectra. Peaks at 950 nm indicate emission from the 3D material, and peaks at 700 nm can be associated with the LPK. Reproduced with permission.[181] Copyright 2019, Wiley-VCH.

Using time-resolved PL, they observed that the addition of the LPK increased the PL lifetime significantly (**Figure 11**c), which was interpreted to be due to a decrease in non-radiative recombination in the material due to the presence of fewer traps. Several other studies have also identified passivation effects using similar PL analysis.[14]

In PL measurements, the strength of the observed signal is given by the efficiency of the light emission processes that occur after photoexcitation. Although non-radiative processes cannot produce their own PL signatures, their effects on radiative processes can be observed. As measurements of non-radiative processes are thus indirect, care must be taken in their analysis to properly identify them. As such, an additional technique is often needed to confirm PL results. For example, Cho et al. compared pristine $Cs_{0.1}FA_{0.74}MA_{0.13}PbI_{2.48}Br_{0.3}$ (CFMPbI) perovskite device with a device layered perovskite $(PEA)_2PbI_4$ layered on CFMPbI (L-CMFPbI) with a mesoporous architecture—fluorine-doped tin oxide/compact and mesoporous TiO_2/perovskite (3D then on top LPK)/spiro-OMeTAD/gold. Using time-resolved PL measurements, they suggested that the faster quenching of the film with the LPK on top is due to the interfacial hole transfer from the 3D layer and the LPK layer, which results in reduced charge carrier recombination as confirmed by impedance spectroscopy.[125]

4.6. Microscopy Techniques

There are many options for studying the charge carrier dynamics in metal halide perovskites, however, these techniques lack spatial resolution in their standard configurations. Spatial resolution is important because perovskite thin films are polycrystalline and optoelectronic properties are not uniform across grains and grain boundaries. For example, it is generally understood that the recombination rate and therefore the diffusion length is influenced by the defect density.[177] These defects can reside in the grain boundaries of the material and act as recombination sites,[178] and there is a link between the passivation of grain boundaries to better performance and stability of perovskite-based devices.[179]

Luckily, many of the time-resolved techniques can be adapted for microscopy to gain spatial resolution in addition to temporal resolution. For example, transient absorption microscopy has been used to elucidate the charge-carrier dynamics of layered perovskites. Deng et al. used transient absorption to investigate exciton diffusion and annihilation in $(BA)_2(MA)_{n-1}Pb_nI_{3n+1}$ thin films with n = 1–5.[152] Overall, they found that the exciton diffusion constant increases with the quantum-well thickness from 0.06 ± 0.03 for n = 1 to 0.34 ± 0.03 cm^2 s^{-1} for n = 5 demonstrating that excitons can diffuse over hundreds of nanometres and across grains in higher n-value materials. Similarly, Toda et al. used ultra-low frequency polarized microscope Raman spectroscopy to visualize grains in the layered perovskite $(PEA)_2PbI_4$ where they were able to study film inhomogeneity.[180]

Confocal time-resolved PL microscopy allows the study of grain boundaries and their effect in charge transport as well as obtaining the diffusion constant of free charges in perovskite films. In this measurement, the crystal is excited at a central point and the time resolved PL is monitored in adjacent pixels at a range of distances, where the rise and decay signal is obtained.[182] By directly visualizing charge transport in this way, Ciesielski et al. showed that grain boundaries can act as "walls" preventing charge transport across grains in the material.[183]

PL microscopy can also be used to study film inhomogeneity, which is important to troubleshoot device fabrication protocols. For example, Ruggeri et al. clearly identified the signatures of phase segregation components in a bilayer 3D/LPK heterostructure (Figure 11). They observed regions with high energy emission (≈700 nm) which corresponds to the LPK areas and other areas with lower energy emission (≈950 nm) which relates to the 3D area of the sample. When looking at PL lifetimes, 3D domains have longer average lifetimes (around 100–200 ns) with respect to the LPK domains (around 30–70 ns). The shorter PL lifetime for the LPK domains could be attributed to the excitonic nature of the layered perovskite, high local excitation densities, and the competing transfer between the LPK and 3D domain.[181]

4.7. Space-Charge Limited Current Measurements

Although it is not a pump/probe technique, space charge limited current (SCLC) measurements should be mentioned due to their ability to derive charge carrier mobility independently of charge density. This is in contrast with time-resolved techniques such as terahertz and microwave spectroscopy that are dependent on mobile charge carriers. SCLC measurements are taken in a simple configuration where the sample is placed between two contacts and the change of current is monitored with applied voltage. The resultant plot is current density (J) versus the voltage (V) where three different regimes are present: i) The Ohmic regime, at low V, where the voltage is proportional to current density (J); ii) the SCLC regime, at higher voltages, where the current becomes space charge limited and there is a quadratic relationship between the current density and voltage ($J \propto V^2$); iii) and the SCLC trap-free regime, at high voltage, when the Fermi level shifts to the valence band of the semiconductor for p-type semiconductors or the traps are filled

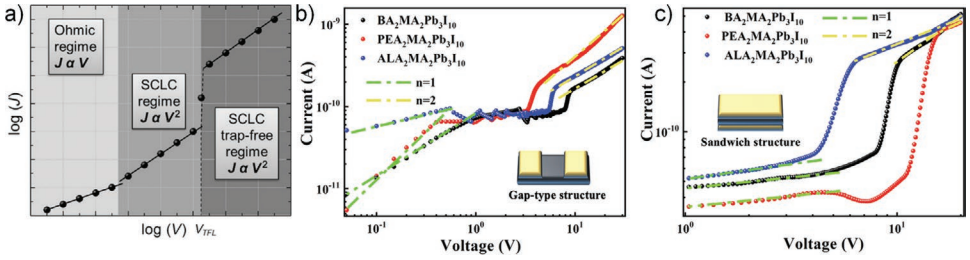

Figure 12. a) Schematic diagram where a sample is sandwiched between electrodes. Reproduced with permission.[184] Copyright 2019, Elsevier B.V. Dark *J*–*V* measurements of hole-only devices in a b) lateral configuration, probing the in-plane mobility, and a c) vertical configuration, probing the out-of-plane mobility, for BA-, PEA-, and ALA-based layered perovskites. Reproduced with permission.[187] Copyright 2020, American Chemical Society.

for n-type semiconductors, this results in an increase in the current density.[184] The inflection point between (ii) and (iii) can be used to characterize the trap density of the studied material.[185] All regions and inflection point are depicted in **Figure 12**a.

One difficulty with using SCLC on perovskite materials is that ion migration can lead to erroneous interpretations of the data. This can be avoided by using pulsed-voltage measurements rather than a simple voltage sweep.[185,186] As ion migration is suppressed in LPKs, however, it should not be as big a factor in analyzing SCLC data for these materials. A good example from Zhang et al. compared the in-plane mobility against the out-of-plane mobility, as shown in Figure 12b,c.[187] Their results clearly show that irrespective of the cation employed, a 3 order of magnitude difference exists between these crystallographic directions, from ≈10^{-2} for in-plane to ≈10^{-5} cm^2 V^{-1} s^{-1} for out-of-plane mobility. Ma et al. investigated the effect of changing the interlayer distance between lead-iodide layers. In this case, mobilities were found to be slightly higher for the shorter interlayer distance, 3.8×10^{-4} cm^2 V^{-1} s^{-1} versus 1.2×10^{-4} cm^2 V^{-1} s^{-1}. This reduced interlayer distance was suggested to increase charge transport due to enhanced orbital interaction between the lead-iodide layers, giving it a partial 3D character.[142]

4.8. Emerging Technologies

There are several exciting emerging technologies that have been implemented for state-of-the-art 3D perovskite materials and have potential for improving the understanding of how LPKs function in devices. As discussed in Section 2.2, structural distortions can alter the exciton binding energy in LPKs. Techniques that can resolve structural information, such as X-ray scattering spectroscopy, time-resolved infrared spectroscopy, and sum-frequency generation have revealed dynamic structural fluctuations in 3D perovskites.[188,189] For example, Guzeturk et al. visualized excitation-induced strain fields in MAPI using X-ray scattering spectroscopy.[188] They correlated these fluctuations with an increased effective carrier mass at early times following photoexcitation, suggesting that carriers initially form polarons and are less mobile.[188] Similar studies of LPKs could help to clarify the relationship between exciton and polaron formation processes and structure and inform materials design.

Multidimensional coherent spectroscopy (MDCS) can be used to measure key interactions such as exciton-phonon coupling in semiconductors such as LPKs and reveal charge transport between heterostructure layers.[190,191] Additionally, it can more clearly disentangle features that spectrally overlap, which is more difficult with traditional one-dimensional techniques, such as TA. It is analogous to a pump/probe technique, except that the pump pulse is divided into two sub-pulses. It is then possible to produce a series time-dependent 2D spectra which are frequency-resolved with respect to both the pump and probe pulses. For $(PEA)_2PbI_4$, MDCS has been used to investigate exciton dephasing rates and the formation of exciton polarons, providing information important for understanding charge transport in the material.[192–194]

5. Layered Perovskites in Devices

LPKs have been established as a clear winning strategy to increase the stability of PSCs, yet their use in devices is complicated due to restricted charge transport. This leads to device efficiencies that are well below those of 3D analogues. An outstanding effort has been made to address this through the engineering of the device structure and molecular engineering of the organic layer.[51,54,168,169,195,196] As such, this section of the review begins with an overview of the basic optoelectronic properties of layered perovskites before discussing the main strategies for engineering PSCs, with a focus on the development of new functional spacers that enhance charge transport.

5.1. Basic Optoelectronics Properties

In a photovoltaic device, light absorbed by the perovskite active layer must be efficiently converted to charge carriers (e.g., electrons and holes or excitons), which must then be separated and selectively move to the electrodes to generate electricity. The perovskite layer must have a favorable combination of optoelectronic properties including strong optical absorption, high charge-carrier mobilities, and long charge-carrier lifetimes for these processes to occur efficiently. An important metric, which combines some of these properties, is the charge-carrier diffusion length L_D,[168,197] which is a function of the diffusion constant D and the total charge-carrier recombination rate R_{total} as follows:

$$L_D(n) = \sqrt{\frac{D}{R_{total}(n)}} \quad (1)$$

The total recombination rate is dependent on the charge-carrier density and can be expressed as:

$$R_{\text{total}} = -\frac{1}{n}\frac{dn}{dt} = n^2 k_3 + nk_2 + k_1 \quad (2)$$

where k_1, k_2, and k_3 are rate constants for monomolecular, bimolecular, and third-order Auger recombination processes, respectively. Additionally, the diffusion constant is related to the charge-carrier mobility μ as:

$$D = \mu k_B T / e \quad (3)$$

where k_B is the Boltzmann constant, T is temperature, and e is the elementary charge. Perovskite layers in devices need only be on the order of a few hundred nanometers thick due to high optical absorption coefficients. The diffusion length criteria are easily satisfied for 3D perovskites, which have average diffusion lengths on the order of microns, however this decreases drastically in LPKs.[168,196]

5.1.1. Charge-Carrier Dynamics

Due to their influence on both charge-carrier diffusion length and quantum efficiency, charge-carrier dynamics are essential for understanding device behavior. In 3D perovskites, charge-carrier dynamics are typically modelled with a simple rate equation, where the rate of change in the charge-carrier density dn/dt is given in terms of the charge-carrier generation rate $G(n)$ and the rate constants for recombination processes k_1, k_2 and k_3.[168] Due to the different dependencies on the initial charge-carrier density, the importance of these processes will vary depending on specific device applications.

$$\frac{dn}{dt} = G(n) - k_3 n^3 - k_2 n^2 - k_1 n \quad (4)$$

Monomolecular recombination in 3D perovskites is typically the result of recombination with defect states or traps and is thus an extrinsic property of the materials and can generally be improved through the optimization of processing. Due to its predominance at lower charge carrier densities, monomolecular recombination is one of the most significant deactivation processes for both photovoltaic and light emission applications.[198] It is generally a non-radiative process,[198] although there are exceptions for highly doped materials.[52] At ambient temperatures, values of k_1 for the most efficient 3D materials range from $\approx 1 \times 10^7$ s^{-1} to 1×10^6 s^{-1}, corresponding to charge-carrier lifetimes (assuming negligible influence of k_2 and k_3) of 100 s of nanoseconds to microseconds.[168]

For layered perovskites with $n = 1$, monomolecular recombination rates are orders of magnitude faster than their 3D counterparts. PL measurements estimate k_1 to be on the order of 10^9 s^{-1} for the common $PEAPbI_4$ structure[81] and are consistent with transient absorption measurements of $BAPbI_4$.[152] Unlike in 3D perovskites, these increased k_1 values are not necessarily an indication of increased trap density, as polaron formation, radiative exciton recombination, and exciton self-trapping are also monomolecular processes.[153,154,199] While the formation of polarons or excitons will limit charge-carrier mobility, it will not deactivate charges in the same way as trap-assisted recombination.

For $n > 1$ layered perovskites, where the exciton binding energy is lower, the monomolecular recombination rates are less dominated by excitonic effects, and defect contributions can become important. For instance, in a series of lead-iodide based mixed PEA/MA thin films, monomolecular recombination rates have been shown to decrease up to 50% added PEA ($n = 3$), contrary to what would be expected due to their increased binding energy. This decrease is likely due to a passivation effect, where inclusion of the organic spacer cations decreases the overall defect density in the material. At compositions greater than $n = 3$, however, exciton recombination begins to dominate the monomolecular recombination dynamics as expected.[52] Similarly, an increasing rate of monomolecular recombination with decreasing n value was observed for BA/MA mixed perovskites[152] across all compositions, consistent with increased exciton recombination. The absence of any clear passivation effects is likely due to better overall phase purity for this series compared to the PEA study.

The source of defects in perovskite materials including layered perovskites is a topic of great interest due to their influence on device efficiency.[198] For instance, Lin et al. found that ion migration was suppressed in a $(BA)_2(MA)_3Pb_4I_{13}$ ($n = 4$) thin film, which could be an indication of decreased defect density in this material as compared to its 3D analogue.[200] Yet, DFT calculations on $(BA)_2(A)Pb_2I_7$, where A = MA, FA, GA, or dimethylammonium (DMA)[201] suggest that increasing the size of the A-site cations induces structural changes analogous to exerting negative pressure on the lattice and results in increased monomolecular recombination rates. These observations, which are supported by TA microscopy, suggest an increased trap concentration or increased phonon-assisted non-radiative recombination.

In 3D perovskites, bimolecular recombination is a result of radiative, electron–hole recombination that has been modelled as an inverse absorption process, like standard semiconductors such as GaAs.[202] Therefore, it is an intrinsic property of the material that should only be sensitive to changes in the band structure. As with monomolecular recombination, the investigation of bimolecular recombination in LPKs is more challenging since it can include a range of processes including electron–hole recombination of excess free charge-carriers and exciton-exciton annihilation.[81,151,152] Accordingly, values of k_2 reported in the literature for $n = 1$ materials vary over several orders of magnitude from 0.2×10^{-9} cm^3 s^{-1} for optical pump/THz probe measurements[81] to $17 \pm 5 \times 10^3$ cm^2 s^{-1} for transient absorption measurements.[152] Due to the importance of these phenomena for dictating the efficiency of devices, more systematic work is needed to resolve these differences and better understand the true nature of bimolecular recombination.

Auger recombination encompasses a range of third order, typically non-radiative processes. The least studied of the various charge-carrier recombination processes, it is most prominent at high charge-carrier densities due to it n^3 dependence, thus imposing an upper limit on the radiative efficiency.[168]

5.1.2. Charge-Carrier Mobilities

An increase in exciton binding energy also has implications for charge-carrier mobility. Effective mobilities in $n = 1$ layered perovskites are comparable to low mobility semiconductors, such as, organic semiconductors, which typically have values of ≈1 $cm^2\ V^{-1}\ s^{-1}$ or lower.[203] Microwave conductivity and THz spectroscopy measurements have established a lower limit of 0.5 and 1 $cm^2\ V^{-1}\ s^{-1}$ for typical LPK thin films,[81] although exciton diffusivity measurements suggest that the exciton mobility could be as high as 7.5 $cm^2\ V^{-1}\ s^{-1}$.[83,130,152] This limits the charge-carrier diffusion lengths in $n = 1$ LPKs to ≈100 nm or less, making them largely unsuitable for use as the sole active layer in standard bilayer photovoltaic devices. In addition to the constraints imposed on the mobility by excitons, charge-carrier mobilities are intrinsically limited by strong electron- or exciton-phonon coupling as they are in 3D perovskites.[160,193] In fact, phonon coupling was found to be so strong that the formation of polarons has been investigated in both layered and 3D perovskites.[153,192,204]

LPKs have also been shown to possess a large mobility anisotropy, where the mobility is larger within the layers of metal halide octahedra than across the insulating layers formed by the spacer cations.[27,81] Recent results show two to three orders of magnitude difference in charge transport efficiency in-plane versus out-of-plane, as suggested by TRMC and photoconductivity data on $(PEA)_2PbI_4$ monocrystals.[129,205] This presents an additional challenge for the fabrication of LPK devices, as the materials tend to assemble parallel to the substrate therefore preventing the efficient diffusion of charges toward the electrodes.

5.2. Single Perovskite Junction Solar Cell Architectures

In the simplest solar cell configuration, analogous to what is implemented for 3D perovskites, the layered material acts as the light absorber layer and is stacked between a hole transport layer and electron transport layer, as shown in **Figure 13**a. Immediately, it is clear that the large bandgap nature of layered perovskites, typically above 2 eV, leads to low current densities due to poor photon harvesting throughout the solar spectrum.[70,206] Additionally, the short charge-carrier diffusion length limits the thickness of the photoactive layer, whilst the high exciton binding energy precludes efficient generation of charges. Accordingly, the first examples of $n = 1$ PSCs showed short-circuit current (J_{SC}) as low as 0.06 mA cm^{-2} and a corresponding PCE of 0.01%.[206] This was subsequently improved to almost 4% PCE by optimizing the charge transport in 2D materials through the engineering of the spacer cation,[56,70,207] yet still well below the efficiencies of >25% reported for solar cells based on 3D perovskites.

A number of strategies have evolved in recent years in an effort to overcome these limitations including utilizing $n > 1$ layered materials, orienting the films for favorable charge transport, mixing layered and 3D materials, and forming heterostructures with layered and 3D materials. All these strategies seek to improve charge transport through increasing the charge-carrier mobility and reducing the "2D" character of the material.

5.2.1. Utilizing n > 1 Materials

At low $n > 1$ values, the perovskite preserves most of the stability whilst the optoelectronic properties resemble more their 3D counterparts with the increase of n (Figure 13b).[16] Most importantly, this includes bandgap narrowing, decrease of exciton binding energy and enhanced charge transport, as discussed in more detail in Section 2. For materials with n up to 4, phase-pure PSCs are reported reaching over 11% efficiency[13] along with excellent long-term (>3000 h) stability in humidity and

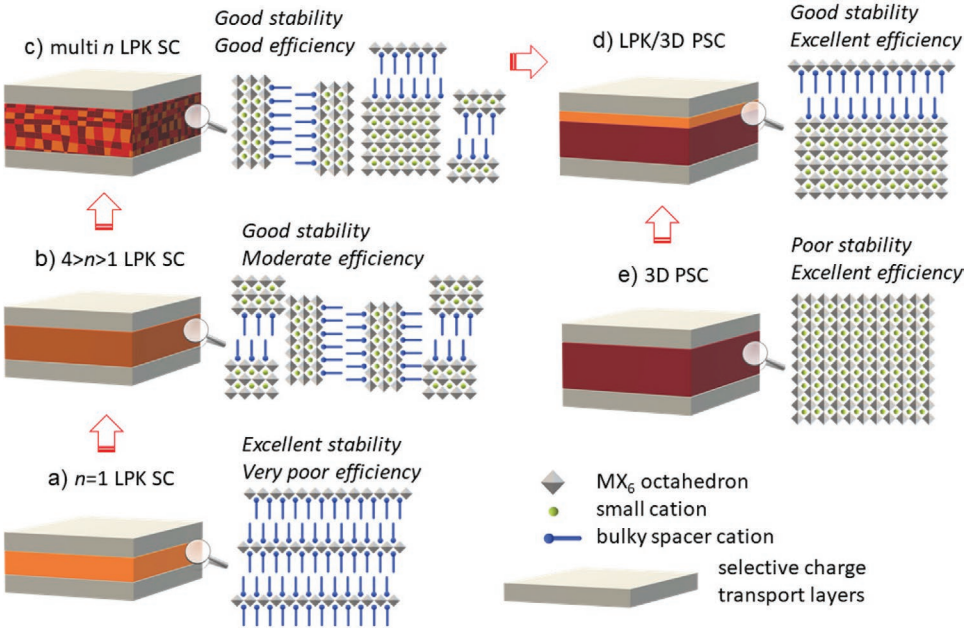

Figure 13. Schematic representation of PSC architectures with the focus on the structure and ordering in the perovskite layer.

illumination tests. The higher current density is the result of a lower bandgap and an increased charge diffusion length. This allows for better coverage of the solar spectrum and increased film thickness that enhances the photons harvesting.

For large n-values, the layered perovskite optoelectronics are essentially indistinguishable from their 3D counterpart. Efficiencies over 19% were reached for $n > 4$ PSCs,[14,208] but so does the stability resemble more the 3D perovskites (Figure 13c).[83,87] Additionally, as described in Section 2.3, it is difficult to synthesize phase pure $n > 1$ LPKs,[78] and the concomitant presence of phases with different n can lead to a cascade of energy and charge transfer events, as depicted in **Figure 14**a.[79,85,209–211] In $(BA)_2(MA)_{n-1}Pb_nI_{3n+1}$ films (nominally $n = 4$), this charge transfer was found to facilitate the separation of electrons and holes to different surfaces of the film, which is potentially a benefit for solar devices.[79] Furthermore, careful control of small-to-large n-phases distribution can be used to improve light-harvesting through photon recycling.[166,212,213] However, the presence of multi-n regions can also lead to a disordered system where trap states can result in nonradiative charge recombination and thus lower efficiencies.[214]

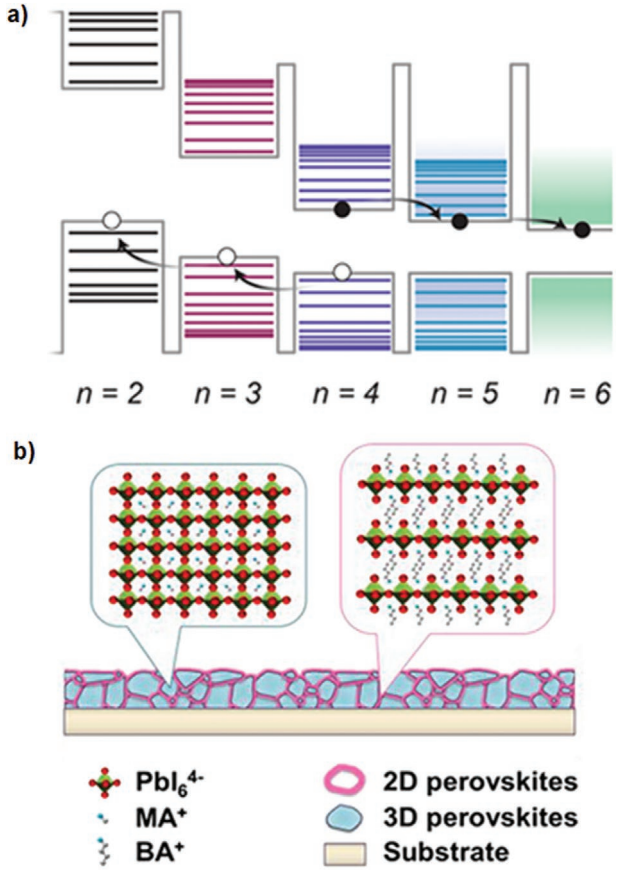

Figure 14. a) Schematic of the energy level alignment for mixed low-n LPKs. After photoexcitation and exciton dissociation, electrons will transfer from low- to high-n, while the opposite occurs for holes. Reproduced with permission.[214] Copyright 2018, American Chemical Society. b) Schematic of the perovskite film treated by BA to form a 2D/3D stacking structure that resembles brick and mortar, with the 3D structure and the layered perovskite zoomed in as insets. Reproduced with permission.[220] Copyright 2018, American Chemical Society.

An option to overcome charge transport limitations is to take advantage of the anisotropic charge mobility in LPKs. Here, charge transport is more efficient within the inorganic layers than across the organic layers.[215,216] Therefore, orienting the crystals so the lead octahedra planes are "vertically oriented" leads to improved charge collection as charges do not need to cross organic layers to reach the extraction contacts. Unfortunately, this is difficult to achieve for low n-phases.[217] A successful illustration of this approach is the MACl addition to $(ThMA)_2(MA)_2Pb_3I_{10}$, that was shown to promote the formation of strongly (111) and (202) oriented films and yielded record PCEs of over 15%.[218] Nonetheless, these values are still well below the Shockley–Queisser limit (≈16% for a bandgap of 2.3 eV and up to 30% for 1.6 eV) and significantly lower than the 3D counterparts.[218,219]

5.2.2. Mixing of 3D and Layered Materials

A mixture of low and high n, that is, "2D" like areas embedded within "3D"-like areas can combine the stability of LPKs with the high mobilities and long charge-carrier lifetimes of 3D perovskites, as shown in Figure 14b.[87,220] For example, Wang et al. investigated the effect of incorporating BA cations into the 3D perovskite $FA_{0.83}Cs_{0.17}Pb(I_yBr_{1-y})_3$ and observed the formation of LPK "platelets" between the 3D grains in the film (Figure 10A).[14] This incorporation does not significantly alter the absorption spectrum of the underlying 3D material; however, suppression of the non-radiative recombination in the highly crystalline material through addition of LPK "platelets" is proposed to result in higher PCEs (17.2% vs 15.2%), faster power stabilization (5 s vs 15 s), and a lower hysteresis. In a similar example, Li et al. have seeded the 3D perovskite precursor solution with 3 mol% $EDBEPbI_4$ microcrystals to obtain a composite consisting of phase-pure $n = 1$ DJ-phase that passivate the 3D phase.[221] The reduced trap densities, as compared to the 3D-only perovskite, lead to a record DJ phase PCE of up to 21% along with an excellent device shelf life, for example, 90% PCE was retained over 1000 h in 65% humidity storage conditions.

5.3. Layered Hybrid Perovskite/3D Perovskite Heterojunction Solar Cells

More recently, Docampo et al. have proposed a different solar cell architecture that takes full advantage of both the layered and the 3D materials, as pictured in Figure 13d.[15] The use of layered perovskite in combination with an archetypal 3D perovskite in the LPK/3D bilayer heterojunction has proven to be an excellent strategy for high efficiency PSCs with PCE over 23% and outstanding stability.[126,222,223] The heterojunction approach consists of depositing a thin LPK layer between the 3D perovskite and the selective charge transport material. This is normally achieved via a cation exchange reaction on the surface of a predeposited 3D layer, although a one-step deposition method can also be used. In either arrangement, the introduction of the LPK interlayer increases the potential for further losses due to either less efficient charge transport in the layered material, inefficient charge transfer across the heterojunction due to poorly matched energy

levels or charge recombination through defects at the interface. All these processes can reduce PSC performance and need to be addressed; wilst the first two are typically associated with poor J_{SC} and fill-factor (FF),[224] charge recombination at interfaces have been linked to reduction of V_{OC}.[225]

5.3.1. Interface Engineering

Charge collection and recombination in solar cells is strongly influenced by the defects at poorly matched interfaces and atomically sharp epitaxial junctions are required to reach the Shockley-Queisser performance limits.[226,227] In this light, layered perovskites have a natural passivating effect on the 3D perovskites and the LPK interfacial layer has consistently been shown to reduce the surface defects, thus decreasing nonradiative, monomolecular recombination.[228,229] However, Hailegnaw et al. show that there is still room for improvement where an estimated loss of ≈0.14 V in the open circuit voltage was assigned to nonradiative recombination at the interface between the 3D and LPK layers.[225]

The contacting interface in the 3D perovskite, I or PbI, and its van der Waals interaction with the LPK layer are critical in determining the electrical properties and charge transfer characteristics of the LPK/3D heterojunction. The first-principle calculation study done by Liu et al. predicts an enhanced carrier separation at the LPK/I interface due to a more favorable built-in electric field in the space-charge region, along with a higher interface bandgap of 1.15 eV, as compared to the LPK/PbI interface (0.53 eV).[228] Additionally, the LPK/I structure has the recombination center located on the LPK side of the interface with a lower density of photocarriers, thus suggesting a reduced rate of charge recombination.

LPK/3D interfaces can undergo dynamical structural mutation due to ion migration across the interface, thus affecting its stability and optoelectronic characteristics. Sutanto and others have experimentally shown that MA cations in the 3D perovskite can migrate into the $n = 1$ LPK, which acts as an "ion scavenger," resulting in formation of $n > 1$ phases.[17,230] Although, the reason why 2-thiophenethylammonium spacer blocks the migration of small cations is not clear, one possible explanation is the stronger intramolecular interactions that rigidifies the organic interlayer, as supported by work of Shi et al.[131]The rigid π-conjugated cation, bithiophenylethylammonium 2T, is shown to reduce disorder at the interface and lower halide vacancy concentration, thereby strongly reducing the I-Br interdiffusion and enabling access to stable epitaxial heterostructures.[131] However, more work is required to fully understand and control the underlaying mechanisms; specifically, the role of highly conjugated organic spacers in determining the stability and electronic properties of interfaces.

5.3.2. Energy Level Engineering

As LPK materials generally have wider bandgap than their 3D counterparts, careful tuning of the VB and conduction bands (CB) can be used to control interfacial charge transfer. Tuning the VB above that of the 3D layer allows an efficient extraction of holes, whilst its higher CB blocks electron transfer, thereby resulting in selective charge extraction that potentially avoids the use of costly and inefficient organic HTMs.[231] Initial results show good progress over interfacial charge transfer dynamics through, for example, simple fluorination of the aromatic spacers that can reduce the VB by 0.5 eV.[232–234] The use of the fluorinated cation FEA was shown to result in an enhanced interfacial hole extraction and suppression of undesired phases that contribute to PCEs over 22%.[115]

5.4. Functional Spacer Cations for Enhanced Charge Transport

The main bottleneck to the LPK-based high-performance PSCs is inefficient charge transport, caused by quantum and dielectric confinement.[235,236] The charge carrier mobility is not only low compared to the 3D counterpart, but is also anisotropic, that is, more efficient within the metal halide plane (in-plane) than across the organic layer (out-of-plane).[79,236] This is further exacerbated by the typical 'horizontal' crystallization of LPK films, greatly reducing the conductivity between electrodes and, thereby, the photovoltaic efficiency in standard device configurations.[78,218]

In order to maximize the potential of LPK-based devices, it is therefore critical to understand the physical and chemical reasons underlying poor charge transport. Here, if we consider the charge transport between inorganic layers as a tunneling process mediated by the organic interlayer shown in **Figure 15**a,[237,238] then the two properties of the junction controlling the tunneling probability are the barrier width and height.[239–241] Whilst the former can be adjusted through the size of the spacer cation, the barrier energy height depends both on the energetic alignment between the inorganic and organic layers,[19,239,242] and the degree of intermolecular electronic coupling between the neighboring organic cations.[19,142,216,243] Several approaches directed toward enhancing the charge transport across the organic layer are currently emerging, as illustrated in Figure 15b, and discussed below.

5.4.1. Barrier Width

Enhanced out-of-plane charge transport is expected with a reduction of the distance between the metal halide layers as is the case for established quantum well systems such as GaAs/InGaAs/GaAs.[244] This is indeed the case for linear aliphatic spacers with varied length, as shown by Li et al. Here, both in-plane and out-of-plane charge carrier mobility clearly increases with the reduction of interlayer distance, with the exception of BA_2PbI_4.[18] From the series of n-alkyl cations, Li et al. found hexylammonium HA to show the highest in-plane (1.5 $cm^2\ V^{-1}\ s^{-1}$) and out-of-plane mobility ($3 \times 10^{-4}\ cm^2\ V^{-1}\ s^{-1}$) due to the combination of low interlayer distance and non-distorted carbon chain, as further discussed in below.[18] For LPKs based on aromatic spacers SCLC measurements also show a trend of increase in both hole and electron mobilities with the reduction in d-spacing.[245] Although not clearly specified, the device architecture and crystal orientation suggest that it is the out-of-plane mobility

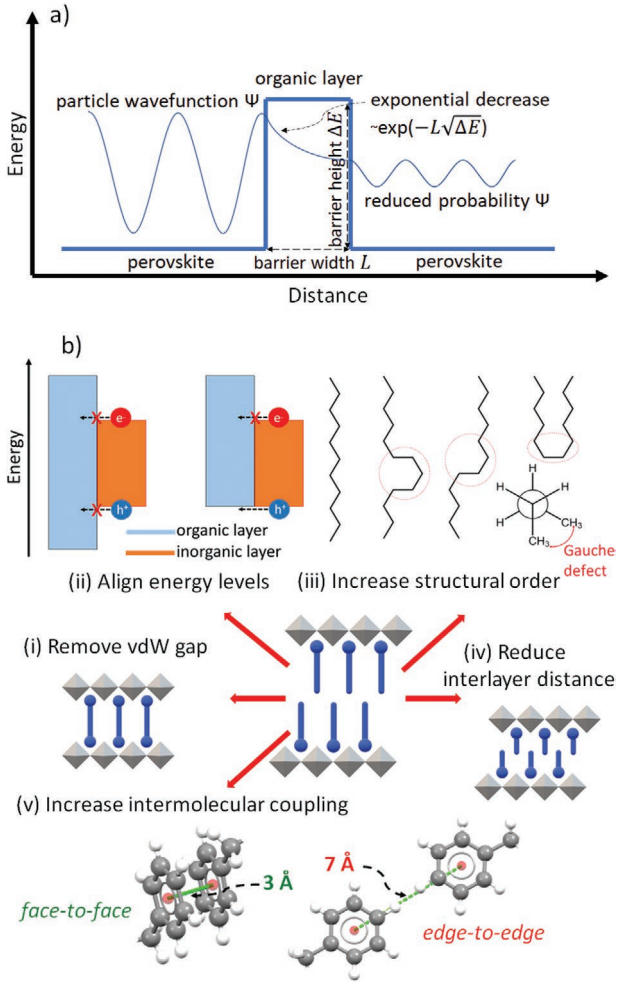

Figure 15. a) Schematic representation of particle tunneling through a potential barrier. b) Summary of experimentally proven or theoretized strategies toward increasing the charge transport in LPK materials: i) Removal of the vdW gap (DJ phase); ii) aligning the energy levels of the inorganic and organic layers (extended π-conjugation, inorganic lattice distortion, halide content); iii) increasing the structural order in the organic layer (rigid spacers, intermolecular π-π, π-cation interactions, H-bonds, vdW forces); iv) reduction of the interlayer distance (short spacers, DJ phase); v) increasing the intermolecular coupling (coaligned face-to-face stacking, reduced vdW gap).

being reported. Interestingly, the hole mobility of about 2×10^{-4} cm^2 V^{-1} s^{-1} obtained for the shortest barrier length of 1.4 nm is quite similar to the above discussed study by Li et al.,[18] whilst the electron mobility is consistently one order of magnitude lower.

It is important to note that the nature of the cation plays a role in defining charge carrier mobility and care must be taken to select appropriate systems to compare. For instance, one of the very few studies looking into the out-of-plane electron mobility reports a lower value measured by TRMC for $(BA)_2PbI_4$ with a shorter d-spacing of 13.76 Å, as compared to $(PEA)_2PbI_4$ with 16.35 Å spacing.[216] In this case, the change in mobility values are most likely caused by the very different nature of cations, that is, aromatic versus aliphatic rather than the change in interlayer distance.

Because the distance between the two inorganic layers is normally smaller in the DJ phase than in the RP phase,[27]its use is promising from the point of view of improving charge transport. Additionally, this avoids the disruption of electronic coupling in the interlayer as one spacer cation can form a continuous link between the inorganic layers.[35] Theoretical work by Ghosh et al. on the 3-(aminomethyl)piperidinium (3AMP) based DJ phase, predicts halogen–halogen electronic coupling between the lead halide layers, due to the short interlayer distance of 4.15 Å, and enhanced delocalization of band-edge charge densities, especially in the VBM, indicating inhibition of carrier recombination process and enhanced interlayer hole-transport for these types of structures as shown in **Figure 16**.[35,246]

An even smaller interlayer distance of 3.36 Å is obtained for the for $n > 3$ LPKs based on PDMA.[57] Hall effect measurements show p-type behavior with a carrier concentration of 3.00×10^8 cm^{-3} and Hall mobility of 0.75 cm^2 V^{-1} s^{-1} for $n = 10$, comparable to 3D perovskites.[247] The determined electron diffusion length of 800 nm, using intensity-modulated photocurrent spectroscopy and intensity-modulated photovoltage spectroscopy, is again very similar to the 3D counterpart.[247] A separate complementary study by Li and Milic et al. reported a high electron mobility for PDMA-based perovskites, 8.76×10^{-3} cm^2 V^{-1} s^{-1} for $n = 1$.[248] For the thiophene analogue (ThDMA) SCLC measurements show a trap density in the 10^{15} cm^{-3} range with electron and hole mobilities of 1.05×10^{-3} cm^2 V^{-1} s^{-1} and 7.76×10^{-4} cm^2 V^{-1} s^{-1}, leading to a high PCE = 15.75% for the $n = 5$ phase.[249]

Small organic spacers with the positive charge delocalized within the aromatic ring can relax the LPK structure by reducing the distortion of the inorganic layer and reduce the confinement effect.[55,250,251] In this context imidazole, the aromatic five-membered heterocycle, has proven a good alternative to the phenyl analogues, for example, PEA.[55,251] The short spacing distance of 4.149 Å, found for (ImEA)[PbI_4], results in

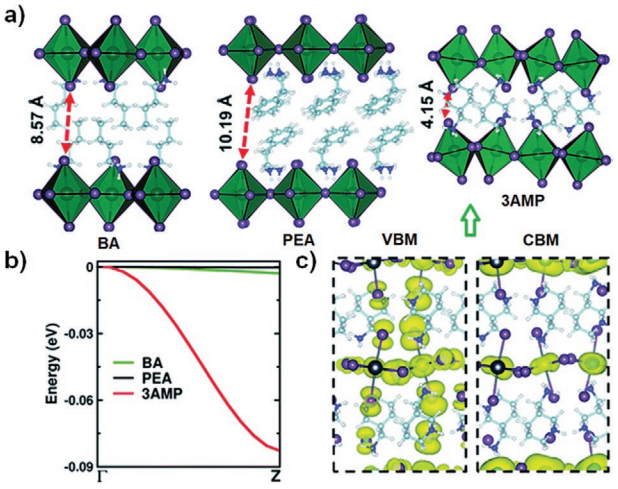

Figure 16. DFT calculated orbital coupling between organic sheets. a) Schematics of the DFT calculated crystal structures formed by employing BA, PEA, and 3AMP as the spacer cation. b) Comparison of valence band dispersion curves along the stacking axis for these 2D-perovskites. c) The electronic charge densities of VBM and CBM for (3AMP)PbI_4. The band edge charge densities are delocalized over the inorganic layer. Reproduced with permission.[35] Copyright 2020, American Chemical Society.

a reduced bandgap and very low excitonic binding energy of 94 meV, as determined from temperature-dependent PL data.[55] The enhanced photoconductivity and reduced trap density allows for incident photon-to-electron conversion efficiencies of up to 60%. Although low when compared to 3D perovskites, this gives one of the highest PCE = 1.83% for solar cells based solely on n = 1 LPK as the light absorbing layer. That said, the highest to date PCE of 3.85% for n = 1 2D perovskites was obtained for a DJ LPK based on the asymmetric alkyl diamine 3-(dimethylammonium)-1-propylammonium DMAPA.[56] Again, this is associated with a reduced confinement resulting from the short interplanar distance of 4.55 Å.

5.4.2. Barrier Height

In commonly used LPKs, the organic layer has a much larger bandgap as compared to the metal halide layer, as illustrated in Figure 3. Matching the energy levels of the two layers could lead to their electronic coupling and should remove the barrier for charge tunneling through the organic interlayer, as shown in Figure 16a, thus enabling higher charge mobilities. In this light, the recent work by Seshadri et al. has shown an order of magnitude increase in conductivity, as measured by TRMC, when replacing the aliphatic BA cation with the aromatic 2-(4-biphenyl)ethylammonium (BPEA) in $(BPEA)_2(MA)Pb_2I_7$.[252]

Numerous reports have emerged on large custom-made organic spacers aimed at controlling the energy and charge transfer events between the inorganic and organic components through the alignment of their energy levels.[205,242,254–256] For example, functionalized tetrathiophene ethylammonium was molecularly engineered (4Tm, 4TCNm, BTm) to allow the formation of LPK structures with the highest occupied molecular orbital and lowest unoccupied molecular orbital levels of the organic spacer close to the CB and VB of the inorganic layer (**Figure 17**a).[242] Here, a higher field-effect hole mobility of 2.32 $cm^2\ V^{-1}\ s^{-1}$ measured for $(4Tm)_2SnI_4$, as compared to 0.15 $cm^2\ V^{-1}\ s^{-1}$ obtained for $(PEA)_2SnI_4$.[257] This supports the idea of charge transport enhancement upon matching the energy levels of the metal halide and organic interlayers. Furthermore, Passarelli et al. showed an impressive four orders of magnitude out-of-plane conductivity increase of up to 10^{-4} S m^{-1} in the series of n = 1 LPKs based on aliphatic < naphthalene << pyrene < perylene spacers, as shown in Figure 17b,c.[19] In this study, the modest PCE of 1.38% reported for $(Pyr\text{-}O\text{-}Prop)_2PbI_4$ is one of the highest amongst LPK-based solar cells with n = 1 and mainly arises from the poor light absorption and thus a low J_{SC} = 2.43 mA cm^{-2}.

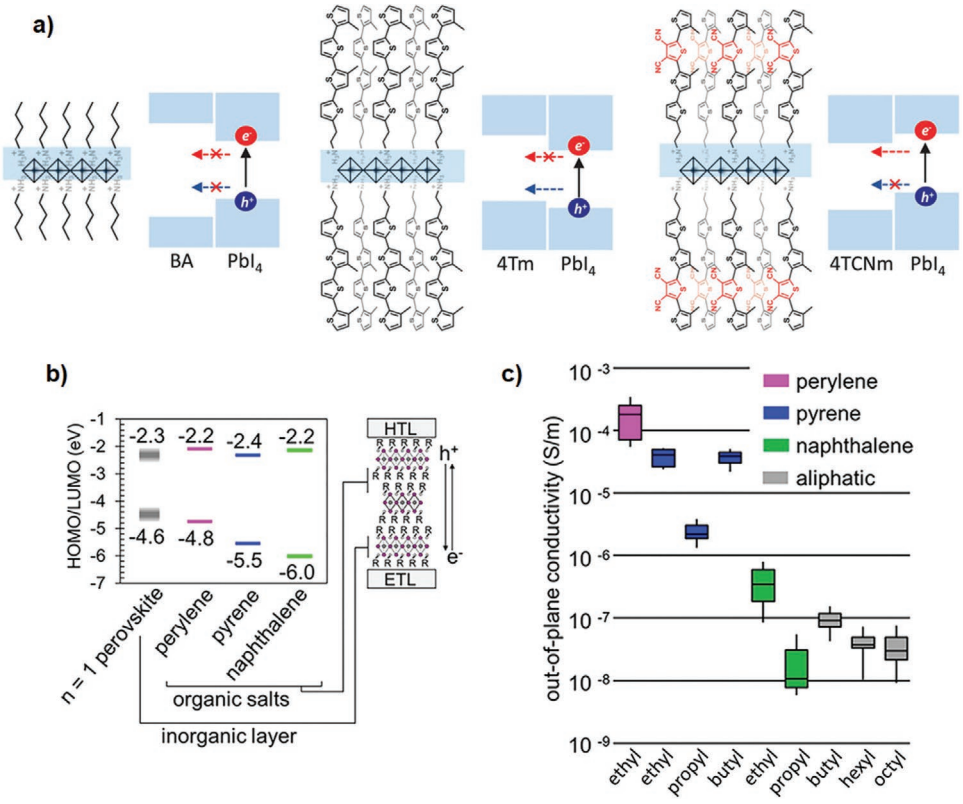

Figure 17. a) Illustration of energy alignment effect on the charge transfer events for three cases of energy band alignment of organic spacer in $(BA)_2PbI_4$, $(4Tm)_2PbI_4$, and $(4TCNm)_2PbI_4$. Reproduced with permission.[253] Copyright 2020, AIP Publishing LLC. Illustration of interplay between the energy alignment, intermolecular interactions, and the out-of-plane conductivity. b) Comparison of energy levels of the inorganic layer n = 1 (gray) and the energy levels of the conjugated organic spacer: Per-*O*-Et, Pyr-*O*-Prop, and Nap-*O*-Prop. c) Out-of-plane conductivity of n = 1 layered perovskites. Higher conductivity is observed for materials based on organic spacers with better energy alignment with the inorganic layer. b,c) Reproduced with permission.[19] Copyright 2018, American Chemical Society.

5.4.3. Intermolecular Coupling

A strong overlap of molecular π-π orbital overlap in the organic layer is necessary for efficient out-of-plane charge transport in LPKs as shown for the field of organic semiconductors.[258,259] This is largely determined in LPKs by the packing motif of the aromatic units which has a strong impact on the out-of-plane conductivity.[19] Passarelli et al. have found that n = 1 LPKs based on naphthalene and pyrene cations with the edge-to-face stacking display a higher conductivity as compared to the more poorly interacting edge-to-edge stacking analogues. Importantly, this work shows that major advances into the charge transport in LPK material are possible by employing extended π-conjugated systems with matched energy levels and careful control of intramolecular π-stacking interactions.

In an attempt to control the packing order of cations in the organic bilayer, simple halogenation of PEA has shown promising results.[68,69,130] In the 2-, 3-,4-fluorination series, the para substitution in 4FPEA shows the highest degree of order in theorganic layer.[68,260,261] Here, the organic cations are packed facing the same direction as shown by the small average phenyl ring centroid–centroid distances.[129] The out-of-plane TRMC-determined mobility of $(4FPEA)_2PbI_4$ is about 7 times larger than that of $(PEA)_2PbI_4$, in line with the idea of stronger orbital coupling in the fluorinated organic interlayer.[216] Interestingly the interlayer distance for FPEA is slightly larger than the PEA based LPK, showing that the orbital coupling is more important for the improved out-of-plane conductivity than the interlayer distance in this case. This results in improved solar cell performance with PCE >13% for $(4FPEA)_2MA_4Pb_5I_{16}$-based PSCs compared to the unmodified PEA analogue with a PCE of 10% or below.[69,232]

In the context of molecular packing, it is important to note that disorder in the organic layer also plays a role in determining the out-of-plane charge mobility. For instance, Li et al. have shown a clear reduction in the effective mobility through OPTP and SCLC measurements in a series of linear aliphatic spacers ($(CH_3(CH_2)_nNH_3)_2PbI_4$, n = 4, 6, 8, 10, 12, 18). The decrease can be linked to the local chain distortion of organic cations,[18] which is explained by the localization and self-trapping of charge carriers in potential wells caused by this disorder.[262,263]

6. Conclusions

LPKs have emerged as a viable solution to address perovskite stability concerns and enable their implementation in wide-scale energy harvesting. Yet, although more stable, the performance of devices incorporating LPKs still lags behind that of state-of-the-art, multi-cation perovskite materials. This is caused by the current iteration of cations used within the organic layer which lead to poor charge transport of the material. On balance, a compromise between efficiency and stability is typically sought, involving careful control of phase purity and distribution, interfaces and energy/charge transfer processes. Further progress is hindered by the difficulty in identifying the fundamental optoelectronic processes in these materials. Here, the high exciton binding energy of LPKs lead to the formation of multiple photoexcited species, which greatly complicate measurement interpretation.

The most popular strategy to mitigate poor charge transport concentrates on introducing more '3D character' to the LPK. This can be achieved for instance by increasing the number of lead halide layers n or by blending LPKs with 3D materials. An alternative strategy focusses on orienting the lead halide octahedra layer of LPKs in the "vertical" direction, that is, avoiding charge transfer across the organic spacer layers. Yet, none of these approaches address the root cause of poor charge transport in these systems. LPKs with varied n exhibit both lower exciton binding energy, which is desirable for efficient charge transport, but lower stability, and a compromise must be sought. Alternatively, a well-defined heterostructure can be engineered by introducing an LPK layer over a 3D perovskite layer. This takes advantage of the high charge transport of state-of-the-art materials, while minimizing the impact of the LPK by making it as thin as possible. Yet, again, a compromise must necessarily be sought, as thinner LPKs negatively impact stability.

Clearly, we must move away from these compromises and address the inherent poor charge transport within the organic spacer layers. A more promising strategy we highlight in this review is to choose spacer cations that promote charge transport through better energetic alignment between the organic spacer and the lead halide octahedra. This should reduce confinement effects for one type of charge carrier and enable the development of selective charge transport layers that do not rely on expensive small molecules. We additionally highlight the importance of well-ordered organic spacers in optimizing both charge transport and stability of the resulting LPKs. Specifically, fluorinated aromatic amines and electron-rich thiophene systems are promising candidates and their effect on the charge transport properties are worth being investigated. We expect more work in this direction to bring better insight into the underlying mechanisms and guide research toward better charge transport in LPKs.

Ultimately, we expect that fully exploring bidentate cations and focus on ordered DJ systems will lead to the desired high efficiency with high stability combination. These materials remove the insulating van der Waals gap present in the more common RP phase and thus achieve more rigid structures with shorter spacing between the lead octahedra layers. This, in turn, allows electronic coupling between the latter, and, therefore, enhanced charge transport without compromising the stability of the structure. We believe this novel approach will open the door to a new generation of stable layered perovskites with high out-of-plane conductivity that can potentially match the performance of 3D systems.

Here, measurements of fundamental optoelectronic properties can help to shed light on device bottlenecks. However, the photoinduced dynamics are complicated due to the variety of photoexcited species that exist at similar time frames. To gain a fuller picture of the mechanisms at play, multiple complementary techniques should be considered together to isolate contributions from different species and remove speculation from the data analysis. For example, visible transient absorption spectra can include contributions from free charge-carriers, excitons, and polarons, but analogous MDCS techniques allows for the identification of coupled species, helping to disentangle these

overlapping features. Furthermore, THz and microwave spectroscopy can selectively target free charge-carriers, and X-ray and IR methods give dynamic structural information.

A clear challenge in the development of LPKs is the near infinite list of potential cation candidates. Ultimately, we need a concerted research effort between the myterials synthesis and characterization communities in order to narrow down this list. We would also like to emphasize here that there are not enough systematic ageing studies of layered materials and devices, with most studies showing simple "storage" tests rather than employing standardized degradation protocols, leading to poor metrics to compare the different structures. It would be beneficial to follow standardized device aging protocols for PSCs.[89] With this, solar cells which take advantage of LPK properties have the potential to reach and surpass efficiencies of 3D materials and bring PSCs one step closer to mass production.

Acknowledgements

D.S. and F.H.B. contributed equally to the work. P.D. and D.S. acknowledge support from the Engineering and Physical Science Research Council through the EP/T010568/1 and EP/S031103/1 projects. F.H.B. acknowledges support from a Doctoral Training Partnership studentship grant from the U.K. Engineering and Physical Sciences Research Council, and R.L.M. acknowledges funding from the University of Warwick.

Conflict of Interest

The authors declare no conflict of interest.

Keywords

charge transport, layered perovskites, perovskite solar cells

Received: December 15, 2020
Revised: March 25, 2021
Published online: May 19, 2021

[1] S. De Wolf, J. Holovsky, S.-J. Moon, P. Löper, B. Niesen, M. Ledinsky, F.-J. Haug, J.-H. Yum, C. Ballif, *J. Phys. Chem. Lett.* **2014**, *5*, 1035.
[2] Y. Yang, Y. Yan, M. Yang, S. Choi, K. Zhu, J. M. Luther, M. C. Beard, *Nat. Commun.* **2015**, *6*, 7961.
[3] H. Eggers, F. Schackmar, T. Abzieher, Q. Sun, U. Lemmer, Y. Vaynzof, B. S. Richards, G. Hernandez-Sosa, U. W. Paetzold, *Adv. Energy Mater.* **2020**, *10*, 1903184.
[4] M. A. Green, E. D. Dunlop, J. Hohl-Ebinger, M. Yoshita, N. Kopidakis, X. Hao, *Prog. Photovoltaics* **2020**, *28*, 629.
[5] M. Li, C. Zhao, Z. K. Wang, C. C. Zhang, H. K. Lee, A. Pockett, J. Barbé, W. C. Tsoi, Y. G. Yang, M. J. Carnie, *Adv. Energy Mater.* **2018**, *8*, 1801509.
[6] A. Al-Ashouri, E. Köhnen, B. Li, A. Magomedov, H. Hempel, P. Caprioglio, J. A. Márquez, A. B. M. Vilches, E. Kasparavicius, J. A. Smith, *Science* **2020**, *370*, 1300.
[7] R. Wang, M. Mujahid, Y. Duan, Z. K. Wang, J. Xue, Y. Yang, *Adv. Funct. Mater.* **2019**, *29*, 1808843.
[8] A. Babayigit, A. Ethirajan, M. Muller, B. Conings, *Nat. Mater.* **2016**, *15*, 247.
[9] K. Dedecker, G. Grancini, *Adv. Energy Mater.* **2020**, *10*, 2001471.
[10] C. Liu, W. Li, J. Fan, Y. Mai, *J. Energy Chem.* **2018**, *27*, 1054.
[11] F. Sani, S. Shafie, H. N. Lim, A. O. Musa, *Mater* **2018**, *11*, 1008.
[12] S. Chen, N. Shen, L. Zhang, L. Zhang, S. H. Cheung, S. Chen, S. K. So, B. Xu, *Adv. Funct. Mater.* **2020**, *30*, 1907759.
[13] H. Tsai, W. Nie, J.-C. Blancon, C. C. Stoumpos, R. Asadpour, B. Harutyunyan, A. J. Neukirch, R. Verduzco, J. J. Crochet, S. Tretiak, *Nature* **2016**, *536*, 312.
[14] Z. Wang, Q. Lin, F. P. Chmiel, N. Sakai, L. M. Herz, H. J. Snaith, *Nat. Energy* **2017**, *2*, 17135.
[15] Y. Hu, J. Schlipf, M. Wussler, M. L. Petrus, W. Jaegermann, T. Bein, P. Müller-Buschbaum, P. Docampo, *ACS Nano* **2016**, *10*, 5999.
[16] I. C. Smith, E. T. Hoke, D. Solis-Ibarra, M. D. McGehee, H. I. Karunadasa, *Angew. Chem.* **2014**, *126*, 11414.
[17] J. Schlipf, Y. Hu, S. Pratap, L. Bießmann, N. Hohn, L. Porcar, T. Bein, P. Docampo, P. Müller-Buschbaum, *ACS Appl. Energy Mater.* **2019**, *2*, 1011.
[18] C. Li, J. Yang, F. Su, J. Tan, Y. Luo, S. Ye, *Nat. Commun.* **2020**, *11*, 5481.
[19] J. V. Passarelli, D. J. Fairfield, N. A. Sather, M. P. Hendricks, H. Sai, C. L. Stern, S. I. Stupp, *JACS* **2018**, *140*, 7313.
[20] H. Kim, M.-J. Choi, J. M. Suh, J. S. Han, S. G. Kim, Q. Van Le, S. Y. Kim, H. W. Jang, *NPG Asia Mater* **2020**, *12*, 21.
[21] N. Liu, P. Liu, H. Zhou, Y. Bai, Q. Chen, *J. Phys. Chem. Lett.* **2020**, *11*, 3521.
[22] Y. Liu, Z. Yu, S. Chen, J. H. Park, E. D. Jung, S. Lee, K. Kang, S.-J. Ko, J. Lim, M. H. Song, *Nano Energy* **2020**, *80*, 105511.
[23] B. Saparov, D. B. Mitzi, *Chem. Rev.* **2016**, *116*, 4558.
[24] R. J. Tilley, *Perovskites: Structure-Property Relationships*, John Wiley & Sons, Hoboken, NJ **2016**.
[25] S. Ahmad, P. Fu, S. Yu, Q. Yang, X. Liu, X. Wang, X. Wang, X. Guo, C. Li, *Joule* **2019**, *3*, 794.
[26] M.-Z. Zhu, C. Li, B. Li, J. Zhang, Y. Sun, W. Guo, Z. Zhou, S. Pang, Y. Yan, *Mater. Horiz.* **2020**, *7*, 2208.
[27] F. Zhang, H. Lu, J. Tong, J. J. Berry, M. C. Beard, K. Zhu, *Energy Environ. Sci.* **2020**, *13*, 1154.
[28] V. M. Burlakov, Y. Hassan, M. Danaie, H. J. Snaith, A. Goriely, *J. Phys. Chem. Lett.* **2020**, *11*, 6535.
[29] M. C. Weidman, A. J. Goodman, W. A. Tisdale, *Chem. Mater.* **2017**, *29*, 5019.
[30] C.-H. Li, M.-Y. Liao, C.-H. Chen, C.-C. Chueh, *J. Mater. Chem. C* **2020**, *8*, 4294.
[31] C. Ortiz-Cervantes, P. I. Román-Román, J. Vazquez-Chavez, M. Hernández-Rodríguez, D. Solis-Ibarra, *Angew. Chem., Int. Ed.* **2018**, *57*, 13882.
[32] K. Yao, X. Wang, F. Li, L. Zhou, *Chem. Commun.* **2015**, *51*, 15430.
[33] K. Yao, X. Wang, Y.-x. Xu, F. Li, L. Zhou, *Chem. Mater.* **2016**, *28*, 3131.
[34] Z. Chen, Y. Guo, E. Wertz, J. Shi, *Adv. Mater.* **2019**, *31*, 1803514.
[35] D. Ghosh, D. Acharya, L. Pedesseau, C. Katan, J. Even, S. Tretiak, A. J. Neukirch, *J. Mater. Chem. A* **2020**, *8*, 22009.
[36] Y. Guo, W. A. Saidi, Q. Wang, *2D Mater.* **2017**, *4*, 035009.
[37] K. Leng, L. Wang, Y. Shao, I. Abdelwahab, G. Grinblat, I. Verzhbitskiy, R. Li, Y. Cai, X. Chi, W. Fu, P. Song, A. Rusydi, G. Eda, S. A. Maier, K. P. Loh, *Nat. Commun.* **2020**, *11*, 5483.
[38] Y. Wang, Y. Shi, G. Xin, J. Lian, J. Shi, *Cryst. Growth Des.* **2015**, *15*, 4741.
[39] Y. Wang, Y.-Y. Sun, S. Zhang, T.-M. Lu, J. Shi, *Appl. Phys. Lett.* **2016**, *108*, 013105.
[40] C. M. M. Soe, G. Nagabhushana, R. Shivaramaiah, H. Tsai, W. Nie, J.-C. Blancon, F. Melkonyan, D. H. Cao, B. Traoré, L. Pedesseau, *Proc. Natl. Acad. Sci. U. S. A.* **2019**, *116*, 58.
[41] C. C. Stoumpos, C. M. M. Soe, H. Tsai, W. Nie, J.-C. Blancon, D. H. Cao, F. Liu, B. Traoré, C. Katan, J. Even, A. D. Mohite, M. G. Kanatzidis, *Chem* **2017**, *2*, 427.

[42] P. Li, C. Liang, X. L. Liu, F. Li, Y. Zhang, X. T. Liu, H. Gu, X. Hu, G. Xing, X. Tao, *Adv. Mater.* **2019**, *31*, 1901966.
[43] H. Gu, C. Liang, Y. Xia, Q. Wei, T. Liu, Y. Yang, W. Hui, H. Chen, T. Niu, L. Chao, *Nano Energy* **2019**, *65*, 104050.
[44] T. Luo, Y. Zhang, Z. Xu, T. Niu, J. Wen, J. Lu, S. Jin, S. Liu, K. Zhao, *Adv. Mater.* **2019**, *31*, 1903848.
[45] C. M. M. Soe, C. C. Stoumpos, M. Kepenekian, B. Traoré, H. Tsai, W. Nie, B. Wang, C. Katan, R. Seshadri, A. D. Mohite, *JACS* **2017**, *139*, 16297.
[46] J.-C. Blancon, A. V. Stier, H. Tsai, W. Nie, C. C. Stoumpos, B. Traore, L. Pedesseau, M. Kepenekian, F. Katsutani, G. Noe, J. Kono, S. Tretiak, S. A. Crooker, C. Katan, M. G. Kanatzidis, J. J. Crochet, J. Even, A. D. Mohite, *Nat. Commun.* **2018**, *9*, 2254.
[47] J. V. Passarelli, C. M. Mauck, S. W. Winslow, C. F. Perkinson, J. C. Bard, H. Sai, K. W. Williams, A. Narayanan, D. J. Fairfield, M. P. Hendricks, *Nat. Chem.* **2020**, *12*, 672.
[48] M. Baranowski, P. Plochocka, *Adv. Energy Mater.* **2020**, *10*, 1903659.
[49] L. M. Herz, *J. Phys. Chem. Lett.* **2018**, *9*, 6853.
[50] D. Marongiu, M. Saba, F. Quochi, A. Mura, G. Bongiovanni, *J. Mater. Chem. C* **2019**, *7*, 12006.
[51] D. B. Straus, C. R. Kagan, *J. Phys. Chem. Lett.* **2018**, *9*, 1434.
[52] R. L. Milot, G. E. Eperon, T. Green, H. J. Snaith, M. B. Johnston, L. M. Herz, *J. Phys. Chem. Lett.* **2016**, *7*, 4178.
[53] V. A. Hintermayr, L. Polavarapu, A. S. Urban, J. Feldmann, *ACS Nano* **2018**, *12*, 10151.
[54] C. M. Mauck, W. A. Tisdale, *Trends Chem.* **2019**, *1*, 380.
[55] B. Febriansyah, T. M. Koh, Y. Lekina, N. F. Jamaludin, A. Bruno, R. Ganguly, Z. X. Shen, S. G. Mhaisalkar, J. England, *Chem. Mater.* **2019**, *31*, 890.
[56] W. Zhao, Q. Dong, J. Zhang, S. Wang, M. Chen, C. Zhao, M. Hu, S. Jin, N. P. Padture, Y. Shi, *J. Mater. Chem. A* **2020**, *8*, 9919.
[57] S. Yu, Y. Yan, M. Abdellah, T. Pullerits, K. Zheng, Z. Liang, *Small* **2019**, *15*, 1905081.
[58] K.-z. Du, Q. Tu, X. Zhang, Q. Han, J. Liu, S. Zauscher, D. B. Mitzi, *Inorg. Chem.* **2017**, *56*, 9291.
[59] J. L. Knutson, J. D. Martin, D. B. Mitzi, *Inorg. Chem.* **2005**, *44*, 4699.
[60] S.-Y. Kim, J.-M. Yang, E.-S. Choi, N.-G. Park, *Nanoscale* **2019**, *11*, 14330.
[61] C. C. Stoumpos, D. H. Cao, D. J. Clark, J. Young, J. M. Rondinelli, J. I. Jang, J. T. Hupp, M. G. Kanatzidis, *Chem. Mater.* **2016**, *28*, 2852.
[62] T. Ishihara, J. Takahashi, T. Goto, *Phys. Rev. B* **1990**, *42*, 11099.
[63] C. Quarti, N. Marchal, D. Beljonne, *J. Phys. Chem. Lett.* **2018**, *9*, 3416.
[64] A. Amat, E. Mosconi, E. Ronca, C. Quarti, P. Umari, M. K. Nazeeruddin, M. Gratzel, F. De Angelis, *Nano Lett.* **2014**, *14*, 3608.
[65] O. J. Weber, K. L. Marshall, L. M. Dyson, M. T. Weller, *Acta Crystallogr., Sect. B: Struct. Sci., Cryst. Eng. Mater.* **2015**, *71*, 668.
[66] M. P. Hautzinger, J. Dai, Y. Ji, Y. Fu, J. Chen, I. A. Guzei, J. C. Wright, Y. Li, S. Jin, *Inorg. Chem.* **2017**, *56*, 14991.
[67] Z. Tang, J. Guan, A. M. Guloy, *J. Mater. Chem.* **2001**, *11*, 479.
[68] J. Hu, I. W. Oswald, S. J. Stuard, M. M. Nahid, N. Zhou, O. F. Williams, Z. Guo, L. Yan, H. Hu, Z. Chen, X. Xiao, Y. Lin, Z. Yang, J. Huang, A. M. Moran, H. Ade, J. R. Neilson, W. You, *Nat. Commun.* **2019**, *10*, 1276.
[69] H. Pan, X. Zhao, X. Gong, Y. Shen, M. Wang, *J. Phys. Chem. Lett.* **2019**, *10*, 1813.
[70] Y. Li, Y. Zhao, H. Cheng, K. Zhao, Z.-S. Wang, *ACS Appl. Mater. Interfaces* **2020**, *12*, 18590.
[71] H. Li, X. Wang, T. Zhang, X. Gong, Q. Sun, H. Pan, Y. Shen, S. Ahmad, M. Wang, *Adv. Funct. Mater.* **2019**, *29*, 1903293.
[72] X. Qi, Y. Zhang, Q. Ou, S. T. Ha, C. W. Qiu, H. Zhang, Y. B. Cheng, Q. Xiong, Q. Bao, *Small* **2018**, *14*, 1800682.
[73] S. Tan, N. Zhou, Y. Chen, L. Li, G. Liu, P. Liu, C. Zhu, J. Lu, W. Sun, Q. Chen, *Adv. Energy Mater.* **2019**, *9*, 1803024.
[74] B. Cheng, T.-Y. Li, P. Maity, P.-C. Wei, D. Nordlund, K.-T. Ho, D.-H. Lien, C.-H. Lin, R.-Z. Liang, X. Miao, I. A. Ajia, J. Yin, D. Sokaras, A. Javey, I. S. Roqan, O. F. Mohammed, J.-H. He, *J. Phys. Commun.* **2018**, *1*, 80.
[75] M. C. Gélvez-Rueda, W. T. Van Gompel, R. Herckens, L. Lutsen, D. Vanderzande, F. C. Grozema, *J. Phys. Chem. Lett.* **2020**, *11*, 824.
[76] W. T. Van Gompel, R. Herckens, K. Van Hecke, B. Ruttens, J. D'Haen, L. Lutsen, D. Vanderzande, *Chem. Commun.* **2019**, *55*, 2481.
[77] L. Zhao, Y. L. Lin, H. Kim, N. C. Giebink, B. P. Rand, *ACS Energy Lett.* **2018**, *3*, 2708.
[78] Y. Hu, L. M. Spies, D. Alonso-Álvarez, P. Mocherla, H. Jones, J. Hanisch, T. Bein, P. R. Barnes, P. Docampo, *J. Mater. Chem. A* **2018**, *6*, 22215.
[79] J. Liu, J. Leng, K. Wu, J. Zhang, S. Jin, *JACS* **2017**, *139*, 1432.
[80] Y. Zhang, P. Wang, M.-C. Tang, D. Barrit, W. Ke, J. Liu, T. Luo, Y. Liu, T. Niu, D.-M. Smilgies, *JACS* **2019**, *141*, 2684.
[81] R. L. Milot, R. J. Sutton, G. E. Eperon, A. A. Haghighirad, J. M. Hardigree, L. Miranda, H. J. Snaith, M. B. Johnston, L. M. Herz, *Nano Lett.* **2016**, *16*, 7001.
[82] X. Wu, M. T. Trinh, X.-Y. Zhu, *J. Phys. Chem. C* **2015**, *119*, 14714.
[83] M. C. Gélvez-Rueda, E. M. Hutter, D. H. Cao, N. Renaud, C. C. Stoumpos, J. T. Hupp, T. J. Savenije, M. G. Kanatzidis, F. C. Grozema, *J. Phys. Chem. C* **2017**, *121*, 26566.
[84] A. Fraccarollo, A. Zoccante, L. Marchese, M. Cossi, *Phys. Chem. Chem. Phys.* **2020**, *22*, 20573.
[85] L. N. Quan, Y. Zhao, F. P. G. d. Arquer, R. Sabatini, G. Walters, O. Voznyy, R. Comin, Y. Li, J. Z. Fan, H. Tan, *Nano Lett.* **2017**, *17*, 3701.
[86] B. E. Cohen, M. Wierzbowska, L. Etgar, *Adv. Funct. Mater.* **2017**, *27*, 1604733.
[87] L. N. Quan, M. Yuan, R. Comin, O. Voznyy, E. M. Beauregard, S. Hoogland, A. Buin, A. R. Kirmani, K. Zhao, A. Amassian, *JACS* **2016**, *138*, 2649.
[88] K. A. Bush, A. F. Palmstrom, Z. Yu, M. Boccard, R. Cheacharoen, J. P. Mailoa, D. P. McMeekin, R. L. Hoye, C. D. Bailie, T. Leijtens, I. M. Peters, M. C. Minichetti, N. Rolston, R. Prasanna, S. Sofia, D. Harwood, W. Ma, F. Moghadam, H. J. Snaith, T. Buonassisi, *Nat. Energy* **2017**, *2*, 17009.
[89] M. V. Khenkin, E. A. Katz, A. Abate, G. Bardizza, J. J. Berry, C. Brabec, F. Brunetti, V. Bulović, Q. Burlingame, A. Di Carlo, *Nat. Energy* **2020**, *5*, 35.
[90] D. T. Gangadharan, D. Ma, *Energy Environ. Sci.* **2019**, *12*, 2860.
[91] B. Kim, S. I. Seok, *Energy Environ. Sci.* **2020**, *13*, 805.
[92] Y. Li, X. Xu, C. Wang, B. Ecker, J. Yang, J. Huang, Y. Gao, *J. Phys. Chem. C* **2017**, *121*, 3904.
[93] G. E. Eperon, S. D. Stranks, C. Menelaou, M. B. Johnston, L. M. Herz, H. J. Snaith, *Energy Environ. Sci.* **2014**, *7*, 982.
[94] Y. Hu, E. M. Hutter, P. Rieder, I. Grill, J. Hanisch, M. F. Aygüler, A. G. Hufnagel, M. Handloser, T. Bein, A. Hartschuh, *Adv. Energy Mater.* **2018**, *8*, 1703057.
[95] N. Pellet, P. Gao, G. Gregori, T. Y. Yang, M. K. Nazeeruddin, J. Maier, M. Grätzel, *Angew. Chem.* **2014**, *126*, 3215.
[96] L. Wang, H. Zhou, J. Hu, B. Huang, M. Sun, B. Dong, G. Zheng, Y. Huang, Y. Chen, L. Li, *Science* **2019**, *363*, 265.
[97] J. M. Frost, K. T. Butler, F. Brivio, C. H. Hendon, M. Van Schilfgaarde, A. Walsh, *Nano Lett.* **2014**, *14*, 2584.
[98] A. M. Leguy, Y. Hu, M. Campoy-Quiles, M. I. Alonso, O. J. Weber, P. Azarhoosh, M. Van Schilfgaarde, M. T. Weller, T. Bein, J. Nelson, *Chem. Mater.* **2015**, *27*, 3397.
[99] M. L. Petrus, Y. Hu, D. Moia, P. Calado, A. M. Leguy, P. R. Barnes, P. Docampo, *ChemSusChem* **2016**, *9*, 2699.
[100] G. Grancini, V. D'Innocenzo, E. R. Dohner, N. Martino, A. S. Kandada, E. Mosconi, F. De Angelis, H. I. Karunadasa, E. T. Hoke, A. Petrozza, *Chem. Sci. J.* **2015**, *6*, 7305.

[101] E. Mosconi, J. M. Azpiroz, F. De Angelis, *Chem. Mater.* **2015**, *27*, 4885.
[102] C.-G. Wu, C.-H. Chiang, Z.-L. Tseng, M. K. Nazeeruddin, A. Hagfeldt, M. Grätzel, *Energy Environ. Sci.* **2015**, *8*, 2725.
[103] J. M. Azpiroz, E. Mosconi, J. Bisquert, F. De Angelis, *Energy Environ. Sci.* **2015**, *8*, 2118.
[104] Y.-C. Zhao, W.-K. Zhou, X. Zhou, K.-H. Liu, D.-P. Yu, Q. Zhao, *Light: Sci. Appl.* **2017**, *6*, e16243.
[105] G. Gregori, T.-Y. Yang, A. Senocrate, M. Grätzel, J. Maier, in *Organic-Inorganic Halide Perovskite Photovoltaics* (Eds: N.-G. Park, M. Gratzel, T. Miyasaka), Springer, Berlin **2016**, p. 107.
[106] J.-W. Lee, S.-G. Kim, J.-M. Yang, Y. Yang, N.-G. Park, *APL Mater.* **2019**, *7*, 041111.
[107] C. Eames, J. M. Frost, P. R. Barnes, B. C. O'regan, A. Walsh, M. S. Islam, *Nat. Commun.* **2015**, *6*, 7497.
[108] L. Liu, S. Huang, Y. Lu, P. Liu, Y. Zhao, C. Shi, S. Zhang, J. Wu, H. Zhong, M. Sui, *Adv. Mater.* **2018**, *30*, 1800544.
[109] H. J. Snaith, A. Abate, J. M. Ball, G. E. Eperon, T. Leijtens, N. K. Noel, S. D. Stranks, J. T.-W. Wang, K. Wojciechowski, W. Zhang, *J. Phys. Chem. Lett.* **2014**, *5*, 1511.
[110] M. De Bastiani, G. Dell'Erba, M. Gandini, V. D'Innocenzo, S. Neutzner, A. R. S. Kandada, G. Grancini, M. Binda, M. Prato, J. M. Ball, *Adv. Energy Mater.* **2016**, *6*, 1501453.
[111] D. Di Girolamo, N. Phung, F. U. Kosasih, F. Di Giacomo, F. Matteocci, J. A. Smith, M. A. Flatken, H. Köbler, S. H. T. Cruz, A. Mattoni, *Adv. Energy Mater.* **2020**, *10*, 2000310.
[112] J. Li, Q. Dong, N. Li, L. Wang, *Adv. Energy Mater.* **2017**, *7*, 1602922.
[113] P. Calado, A. M. Telford, D. Bryant, X. Li, J. Nelson, B. C. O'Regan, P. R. Barnes, *Nat. Commun.* **2016**, *7*, 13831.
[114] S. Bai, P. Da, C. Li, Z. Wang, Z. Yuan, F. Fu, M. Kawecki, X. Liu, N. Sakai, J. T.-W. Wang, *Nature* **2019**, *571*, 245.
[115] Y. Liu, S. Akin, L. Pan, R. Uchida, N. Arora, J. V. Milic, A. Hinderhofer, F. Schreiber, A. R. Uhl, S. M. Zakeeruddin, A. Hagfeldt, M. I. Dar, M. Gratzel, *Sci. Adv.* **2019**, *5*, eaaw2543.
[116] S. Yang, Y. Wang, P. Liu, Y.-B. Cheng, H. J. Zhao, H. G. Yang, *Nat. Energy* **2016**, *1*, 15016.
[117] X. Lian, J. Chen, M. Qin, Y. Zhang, S. Tian, X. Lu, G. Wu, H. Chen, *Angew. Chem., Int. Ed.* **2019**, *58*, 9409.
[118] F. A. Roghabadi, M. Alidaei, S. M. Mousavi, T. Ashjari, A. S. Tehrani, V. Ahmadi, S. M. Sadrameli, *J. Mater. Chem. A* **2019**, *7*, 5898.
[119] K. Domanski, B. Roose, T. Matsui, M. Saliba, S.-H. Turren-Cruz, J.-P. Correa-Baena, C. R. Carmona, G. Richardson, J. M. Foster, F. De Angelis, *Energy Environ. Sci.* **2017**, *10*, 604.
[120] R. García-Rodríguez, D. Ferdani, S. Pering, P. J. Baker, P. J. Cameron, *J. Mater. Chem. A* **2019**, *7*, 22604.
[121] Z. Huang, A. H. Proppe, H. Tan, M. I. Saidaminov, F. Tan, A. Mei, C.-S. Tan, M. Wei, Y. Hou, H. Han, *ACS Energy Lett.* **2019**, *4*, 1521.
[122] J. Chen, D. Lee, N.-G. Park, *ACS Appl. Mater. Interfaces* **2017**, *9*, 36338.
[123] Y. Bai, S. Xiao, C. Hu, T. Zhang, X. Meng, H. Lin, Y. Yang, S. Yang, *Adv. Energy Mater.* **2017**, *7*, 1701038.
[124] J. Chen, J. Y. Seo, N. G. Park, *Adv. Energy Mater.* **2018**, *8*, 1702714.
[125] K. T. Cho, G. Grancini, Y. Lee, E. Oveisi, J. Ryu, O. Almora, M. Tschumi, P. A. Schouwink, G. Seo, S. Heo, *Energy Environ. Sci.* **2018**, *11*, 952.
[126] G. Grancini, C. Roldán-Carmona, I. Zimmermann, E. Mosconi, X. Lee, D. Martineau, S. Narbey, F. Oswald, F. De Angelis, M. Graetzel, M. K. Nazeeruddin, *Nat. Commun.* **2017**, *8*, 15684.
[127] Y. Zhang, Y. Liu, Z. Xu, Z. Yang, S. Liu, *Small* **2020**, *16*, 2003145.
[128] S. Yang, S. Chen, E. Mosconi, Y. Fang, X. Xiao, C. Wang, Y. Zhou, Z. Yu, J. Zhao, Y. Gao, *Science* **2019**, *365*, 473.
[129] H. Li, J. Song, W. Pan, D. Xu, W. a. Zhu, H. Wei, B. Yang, *Adv. Mater.* **2020**, *32*, 2003790.
[130] M. Seitz, A. J. Magdaleno, N. Alcázar-Cano, M. Meléndez, T. J. Lubbers, S. W. Walraven, S. Pakdel, E. Prada, R. Delgado-Buscalioni, F. Prins, *Nat. Commun.* **2020**, *11*, 2035.
[131] E. Shi, B. Yuan, S. B. Shiring, Y. Gao, Y. Guo, C. Su, M. Lai, P. Yang, J. Kong, B. M. Savoie, *Nature* **2020**, *580*, 614.
[132] J. Cho, J. T. DuBose, A. N. T. Le, P. V. Kamat, *ACS Mater. Lett.* **2020**, *2*, 565.
[133] T. Elmelund, R. A. Scheidt, B. Seger, P. V. Kamat, *ACS Energy Lett.* **2019**, *4*, 1961.
[134] K. Leng, I. Abdelwahab, I. Verzhbitskiy, M. Telychko, L. Chu, W. Fu, X. Chi, N. Guo, Z. Chen, Z. Chen, *Nat. Mater.* **2018**, *17*, 908.
[135] Y. Liang, Q. Shang, Q. Wei, L. Zhao, Z. Liu, J. Shi, Y. Zhong, J. Chen, Y. Gao, M. Li, *Adv. Mater.* **2019**, *31*, 1903030.
[136] W. Niu, A. Eiden, G. V. Prakash, J. J. Baumberg, *Appl. Phys. Lett.* **2014**, *104*, 171111.
[137] Y. Shang, Y. Liao, Q. Wei, Z. Wang, B. Xiang, Y. Ke, W. Liu, Z. Ning, *Sci. Adv.* **2019**, *5*, eaaw8072.
[138] P. Li, X. Liu, Y. Zhang, C. Liang, G. Chen, F. Li, M. Su, G. Xing, X. Tao, Y. Song, *Angew. Chem., Int. Ed.* **2020**, *59*, 6909.
[139] H. Wang, Z. Qin, J. Xie, S. Zhao, K. Liu, X. Guo, G. Li, X. Lu, K. Yan, J. Xu, *Small* **2020**, *16*, 2003098.
[140] X. Jiang, J. Zhang, S. Ahmad, D. Tu, X. Liu, G. Jia, X. Guo, C. Li, *Nano Energy* **2020**, *75*, 104892.
[141] F. Li, J. Zhang, S. Jo, M. Qin, Z. Li, T. Liu, X. Lu, Z. Zhu, A. K. Y. Jen, *Small Methods* **2020**, *4*, 1900831.
[142] C. Ma, D. Shen, T. W. Ng, M. F. Lo, C. S. Lee, *Adv. Mater.* **2018**, *30*, 1800710.
[143] S. Ahmad, W. Yu, R. Lu, Y. Liu, T. Jiu, S. Pang, X. Guo, C. Li, *J. Energy Chem.* **2021**, *57*, 632.
[144] W. Ke, L. Mao, C. C. Stoumpos, J. Hoffman, I. Spanopoulos, A. D. Mohite, M. G. Kanatzidis, *Adv. Energy Mater.* **2019**, *9*, 1803384.
[145] L. Cheng, Z. Liu, S. Li, Y. Zhai, X. Wang, Z. Qiao, Q. Xu, K. Meng, Z. Zhu, G. Chen, *Angew. Chem., Int. Ed.* **2021**, *60*, 856.
[146] Y. Chen, Y. Sun, J. Peng, J. Tang, K. Zheng, Z. Liang, *Adv. Mater.* **2018**, *30*, 1703487.
[147] C. Ortiz-Cervantes, P. Carmona-Monroy, D. Solis-Ibarra, *ChemSusChem* **2019**, *12*, 1560.
[148] R. Berera, R. van Grondelle, J. T. Kennis, *Photosynth. Res.* **2009**, *101*, 105.
[149] J. Lauth, S. Kinge, L. D. Siebbeles, *Z. Phys. Chem.* **2017**, *231*, 107.
[150] X. Wu, M. T. Trinh, D. Niesner, H. Zhu, Z. Norman, J. S. Owen, O. Yaffe, B. J. Kudisch, X.-Y. Zhu, *JACS* **2015**, *137*, 2089.
[151] D. Giovanni, W. K. Chong, Y. Y. F. Liu, H. A. Dewi, T. Yin, Y. Lekina, Z. X. Shen, N. Mathews, C. K. Gan, T. C. Sum, *Adv. Sci.* **2018**, *5*, 1800664.
[152] S. Deng, E. Shi, L. Yuan, L. Jin, L. Dou, L. Huang, *Nat. Commun.* **2020**, *11*, 664.
[153] L. Ni, U. Huynh, A. Cheminal, T. H. Thomas, R. Shivanna, T. F. Hinrichsen, S. Ahmad, A. Sadhanala, A. Rao, *ACS Nano* **2017**, *11*, 10834.
[154] F. Thouin, D. A. Valverde-Chávez, C. Quarti, D. Cortecchia, I. Bargigia, D. Beljonne, A. Petrozza, C. Silva, A. R. S. Kandada, *Nat. Mater.* **2019**, *18*, 349.
[155] E. P. Booker, T. H. Thomas, C. Quarti, M. R. Stanton, C. D. Dashwood, A. J. Gillett, J. M. Richter, A. J. Pearson, N. J. Davis, H. Sirringhaus, *JACS* **2017**, *139*, 18632.
[156] D. Cortecchia, S. Neutzner, A. R. S. Kandada, E. Mosconi, D. Meggiolaro, F. De Angelis, C. Soci, A. Petrozza, *JACS* **2017**, *139*, 39.
[157] C. M. Mauck, A. France-Lanord, A. C. Hernandez Oendra, N. S. Dahod, J. C. Grossman, W. A. Tisdale, *J. Phys. Chem. C* **2019**, *123*, 27904.
[158] J. Lloyd-Hughes, T.-I. Jeon, *J. Infrared, Millimeter,Terahertz Waves* **2012**, *33*, 871.
[159] J. A. Spies, J. Neu, U. T. Tayvah, M. D. Capobianco, B. Pattengale, S. Ostresh, C. A. Schmuttenmaer, *J. Phys. Chem. C* **2020**, *124*, 22335.

[160] L. M. Herz, *ACS Energy Lett.* **2017**, *2*, 1539.
[161] Z. Guo, X. Wu, T. Zhu, X. Zhu, L. Huang, *ACS Nano* **2016**, *10*, 9992.
[162] C. L. Davies, J. Borchert, C. Q. Xia, R. L. Milot, H. Kraus, M. B. Johnston, L. M. Herz, *J. Phys. Chem. Lett.* **2018**, *9*, 4502.
[163] C. La-o-vorakiat, H. Xia, J. Kadro, T. Salim, D. Zhao, T. Ahmed, Y. M. Lam, J.-X. Zhu, R. A. Marcus, M.-E. Michel-Beyerle, E. E. M. Chia, *J. Phys. Chem. Lett.* **2016**, *7*, 1.
[164] M. A. Pérez-Osorio, R. L. Milot, M. R. Filip, J. B. Patel, L. M. Herz, M. B. Johnston, F. Giustino, *J. Phys. Chem. C* **2015**, *119*, 25703.
[165] G. Folpini, L. Gatto, D. Cortecchia, M. Devetta, G. Crippa, C. Vozzi, S. Stagira, A. Petrozza, E. Cinquanta, *J. Chem. Phys.* **2020**, *152*, 214705.
[166] S. G. Motti, T. Crjournals, R. Yang, Y. Cao, R. Li, M. B. Johnston, J. Wang, L. M. Herz, *Nano Lett.* **2019**, *19*, 3953.
[167] D. Cheng, Z. Liu, L. Luo, C. Vaswani, J.-M. Park, Y. Yao, Z. Song, C. Huang, D.-H. Mudiyanselage, R. Kim, *J. Chem. Phys.* **2019**, *151*, 244706.
[168] M. B. Johnston, L. M. Herz, *Acc. Chem. Res.* **2016**, *49*, 146.
[169] C. Ponseca Jr., V. Sundström, *Nanoscale* **2016**, *8*, 6249.
[170] W. Rehman, R. L. Milot, G. E. Eperon, C. Wehrenfennig, J. L. Boland, H. J. Snaith, M. B. Johnston, L. M. Herz, *Adv. Mater.* **2015**, *27*, 7938.
[171] Q. Sun, X. Liu, J. Cao, R. I. Stantchev, Y. Zhou, X. Chen, E. P. Parrott, J. Lloyd-Hughes, N. Zhao, E. Pickwell-MacPherson, *J. Phys. Chem. C* **2018**, *122*, 17552.
[172] J. G. Labram, M. L. Chabinyc, *J. Appl. Phys.* **2017**, *122*, 065501.
[173] T. J. Savenije, A. J. Ferguson, N. Kopidakis, G. Rumbles, *J. Phys. Chem. C* **2013**, *117*, 24085.
[174] L. Gao, F. Zhang, X. Chen, C. Xiao, B. W. Larson, S. P. Dunfield, J. J. Berry, K. Zhu, *Angew. Chem., Int. Ed.* **2019**, *58*, 11737.
[175] A. Kumar, A. Solanki, M. Manjappa, S. Ramesh, Y. K. Srivastava, P. Agarwal, T. C. Sum, R. Singh, *Sci. Adv.* **2020**, *6*, eaax8821.
[176] D. P. Millar, *Curr. Opin. Struct. Biol.* **1996**, *6*, 637.
[177] S. D. Stranks, V. M. Burlakov, T. Leijtens, J. M. Ball, A. Goriely, H. J. Snaith, *Phys. Rev. Appl.* **2014**, *2*, 034007.
[178] D. W. de Quilettes, S. M. Vorpahl, S. D. Stranks, H. Nagaoka, G. E. Eperon, M. E. Ziffer, H. J. Snaith, D. S. Ginger, *Science* **2015**, *348*, 683.
[179] T. Niu, J. Lu, R. Munir, J. Li, D. Barrit, X. Zhang, H. Hu, Z. Yang, A. Amassian, K. Zhao, *Adv. Mater.* **2018**, *30*, 1706576.
[180] S. Toda, N. Yanagita, E. Jokar, E. W.-G. Diau, S. Shigeto, *J. Phys. Chem. Lett.* **2020**, *11*, 3871.
[181] E. Ruggeri, M. Anaya, K. Gałkowski, G. Delport, F. U. Kosasih, A. Abfalterer, S. Mackowski, C. Ducati, S. D. Stranks, *Adv. Mater.* **2019**, *31*, 1905247.
[182] K. Handloser, N. Giesbrecht, T. Bein, P. Docampo, M. Handloser, A. Hartschuh, *ACS Photonics* **2016**, *3*, 255.
[183] R. Ciesielski, F. Schäfer, N. F. Hartmann, N. Giesbrecht, T. Bein, P. Docampo, A. Hartschuh, *ACS Appl. Mater. Interfaces* **2018**, *10*, 7974.
[184] K. P. Goetz, O. D. Jurchescu, in *Handbook of Organic Materials for Electronic and Photonic Devices*, Elsevier, **2019**, pp. 453–487.
[185] E. A. Duijnstee, J. M. Ball, V. M. Le Corre, L. J. A. Koster, H. J. Snaith, J. Lim, *ACS Energy Lett.* **2020**, *5*, 376.
[186] V. M. Le Corre, E. A. Duijnstee, O. El Tambouli, J. M. Ball, H. J. Snaith, J. Lim, L. J. A. Koster, *ACS Energy Lett.* **2021**, *6*, 1087.
[187] Y. Zhang, M. Sun, N. Zhou, B. Huang, H. Zhou, *J. Phys. Chem. Lett.* **2020**, *11*, 7610.
[188] B. Guzelturk, T. Winkler, T. W. Van de Goor, M. D. Smith, S. A. Bourelle, S. Feldmann, M. Trigo, S. W. Teitelbaum, H.-G. Steinrück, A. Gilberto, *Nat. Mater.* **2021**, *20*, 618.
[189] F. G. Santomauro, J. Grilj, L. Mewes, G. Nedelcu, S. Yakunin, T. Rossi, G. Capano, A. Al Haddad, J. Budarz, D. Kinschel, *Struct. Dyn.* **2017**, *4*, 044002.
[190] B. Lomsadze, S. T. Cundiff, *IEEE Photonics Technol. Lett.* **2019**, *31*, 1886.
[191] C. L. Smallwood, S. T. Cundiff, *Laser Photonics Rev.* **2018**, *12*, 1800171.
[192] A. R. S. Kandada, H. Li, F. Thouin, E. R. Bittner, C. Silva, *J. Chem. Phys.* **2020**, *153*, 164706.
[193] A. R. S. Kandada, C. Silva, *J. Phys. Chem. Lett.* **2020**, *11*, 3173.
[194] F. Thouin, D. Cortecchia, A. Petrozza, A. R. S. Kandada, C. Silva, *Phys. Rev. Res.* **2019**, *1*, 032032.
[195] Y. Lekina, Z. X. Shen, *J. Sci.: Adv. Mater. Devices* **2019**, *4*, 189.
[196] J. S. Manser, J. A. Christians, P. V. Kamat, *Chem. Rev.* **2016**, *116*, 12956.
[197] N. Ashcroft, N. Mermin, C. T. Stamford, *Solid State Physics* **1976**.
[198] S. D. Stranks, *ACS Energy Lett.* **2017**, *2*, 1515.
[199] J. Yu, J. Kong, W. Hao, X. Guo, H. He, W. R. Leow, Z. Liu, P. Cai, G. Qian, S. Li, *Adv. Mater.* **2019**, *31*, 1806385.
[200] Y. Lin, Y. Bai, Y. Fang, Q. Wang, Y. Deng, J. Huang, *ACS Energy Lett.* **2017**, *2*, 1571.
[201] X. Li, Y. Fu, L. Pedesseau, P. Guo, S. Cuthriell, I. Hadar, J. Even, C. Katan, C. C. Stoumpos, R. D. Schaller, *JACS* **2020**.
[202] C. L. Davies, M. R. Filip, J. B. Patel, T. W. Crjournals, C. Verdi, A. D. Wright, R. L. Milot, F. Giustino, M. B. Johnston, L. M. Herz, *Nat. Commun.* **2018**, *9*, 293.
[203] Y. Yang, Z. Liu, G. Zhang, X. Zhang, D. Zhang, *Adv. Mater.* **2019**, *31*, 1903104.
[204] D. B. Straus, S. H. Parra, N. Iotov, J. Gebhardt, A. M. Rappe, J. E. Subotnik, J. M. Kikkawa, C. R. Kagan, *JACS* **2016**, *138*, 13798.
[205] M. K. Jana, C. Liu, S. Lidin, D. J. Dirkes, W. You, V. Blum, D. B. Mitzi, *Chem. Mater.* **2019**, *31*, 8523.
[206] D. H. Cao, C. C. Stoumpos, O. K. Farha, J. T. Hupp, M. G. Kanatzidis, *JACS* **2015**, *137*, 7843.
[207] M. Safdari, P. H. Svensson, M. T. Hoang, I. Oh, L. Kloo, J. M. Gardner, *J. Mater. Chem. A* **2016**, *4*, 15638.
[208] H. Lai, D. Lu, Z. Xu, N. Zheng, Z. Xie, Y. Liu, *Adv. Mater.* **2020**, *32*, 2001470.
[209] P. Chen, Y. Meng, M. Ahmadi, Q. Peng, C. Gao, L. Xu, M. Shao, Z. Xiong, B. Hu, *Nano Energy* **2018**, *50*, 615.
[210] R. Quintero-Bermudez, A. Gold-Parker, A. H. Proppe, R. Munir, Z. Yang, S. O. Kelley, A. Amassian, M. F. Toney, E. H. Sargent, *Nat. Mater.* **2018**, *17*, 900.
[211] M. Yuan, L. N. Quan, R. Comin, G. Walters, R. Sabatini, O. Voznyy, S. Hoogland, Y. Zhao, E. M. Beauregard, P. Kanjanaboos, *Nat. Nanotechnol.* **2016**, *11*, 872.
[212] R. Yang, R. Li, Y. Cao, Y. Wei, Y. Miao, W. L. Tan, X. Jiao, H. Chen, L. Zhang, Q. Chen, *Adv. Mater.* **2018**, *30*, 1804771.
[213] J. Zhang, J. Qin, M. Wang, Y. Bai, H. Zou, J. K. Keum, R. Tao, H. Xu, H. Yu, S. Haacke, *Joule* **2019**, *3*, 3061.
[214] A. H. Proppe, R. Quintero-Bermudez, H. Tan, O. Voznyy, S. O. Kelley, E. H. Sargent, *JACS* **2018**, *140*, 2890.
[215] W. Fu, J. Wang, L. Zuo, K. Gao, F. Liu, D. S. Ginger, A. K.-Y. Jen, *ACS Energy Lett.* **2018**, *3*, 2086.
[216] F. Zhang, D. H. Kim, H. Lu, J.-S. Park, B. W. Larson, J. Hu, L. Gao, C. Xiao, O. G. Reid, X. Chen, *JACS* **2019**, *141*, 5972.
[217] A. Z. Chen, M. Shiu, J. H. Ma, M. R. Alpert, D. Zhang, B. J. Foley, D.-M. Smilgies, S.-H. Lee, J. J. Choi, *Nat. Commun.* **2018**, *9*, 1336.
[218] H. Lai, B. Kan, T. Liu, N. Zheng, Z. Xie, T. Zhou, X. Wan, X. Zhang, Y. Liu, Y. Chen, *JACS* **2018**, *140*, 11639.
[219] W. Shockley, H. J. Queisser, *J. Appl. Phys.* **1961**, *32*, 510.
[220] Y. Lin, Y. Bai, Y. Fang, Z. Chen, S. Yang, X. Zheng, S. Tang, Y. Liu, J. Zhao, J. Huang, *J. Phys. Chem. Lett.* **2018**, *9*, 654.
[221] P. Li, Y. Zhang, C. Liang, G. Xing, X. Liu, F. Li, X. Liu, X. Hu, G. Shao, Y. Song, *Adv. Mater.* **2018**, *30*, 1805323.
[222] E. H. Jung, N. J. Jeon, E. Y. Park, C. S. Moon, T. J. Shin, T.-Y. Yang, J. H. Noh, J. Seo, *Nature* **2019**, *567*, 511.
[223] C. Ma, C. Leng, Y. Ji, X. Wei, K. Sun, L. Tang, J. Yang, W. Luo, C. Li, Y. Deng, *Nanoscale* **2016**, *8*, 18309.
[224] V. M. Le Corre, M. Stolterfoht, L. P. Toro, M. Feuerstein, C. Wolff, L. n. Gil-Escrig, H. J. Bolink, D. Neher, L. J. A. Koster, *ACS Appl. Energy Mater.* **2019**, *2*, 6280.

[225] B. Hailegnaw, S. Paek, K. T. Cho, Y. Lee, F. Ongül, M. K. Nazeeruddin, M. C. Scharber, *Sol. RRL* **2019**, *3*, 1900126.
[226] B. Ehrler, E. Alarcón-Lladó, S. W. Tabernig, T. Veeken, E. C. Garnett, A. Polman, *ACS Energy Lett.* **2020**, *5*, 3029.
[227] B. Li, V. Ferguson, S. R. P. Silva, W. Zhang, *Adv. Mater. Interfaces* **2018**, *5*, 1800326.
[228] B. Liu, M. Long, M. Cai, L. Ding, J. Yang, *Nano Energy* **2019**, *59*, 715.
[229] Y. Lv, X. Song, Y. Yin, Y. Feng, H. Ma, C. Hao, S. Jin, Y. Shi, *ACS Appl. Mater. Interfaces* **2019**, *12*, 698.
[230] A. A. Sutanto, N. Drigo, V. I. Queloz, I. Garcia-Benito, A. R. Kirmani, L. J. Richter, P. A. Schouwink, K. T. Cho, S. Paek, M. K. Nazeeruddin, *J. Mater. Chem. A* **2020**, *8*, 2343.
[231] T. Zhang, M. Long, M. Qin, X. Lu, S. Chen, F. Xie, L. Gong, J. Chen, M. Chu, Q. Miao, *Joule* **2018**, *2*, 2706.
[232] W. Fu, H. Liu, X. Shi, L. Zuo, X. Li, A. K. Y. Jen, *Adv. Funct. Mater.* **2019**, *29*, 1900221.
[233] C. Liu, J. Sun, W. L. Tan, J. Lu, T. R. Gengenbach, C. R. McNeill, Z. Ge, Y.-B. Cheng, U. Bach, *Nano Lett.* **2020**, *20*, 1240.
[234] Q. Zhou, Q. Xiong, Z. Zhang, J. Hu, F. Lin, L. Liang, T. Wu, X. Wang, J. Wu, B. Zhang, *Sol. RRL* **2020**, *4*, 2000107.
[235] C. Katan, N. Mercier, J. Even, *Chem. Rev.* **2019**, *119*, 3140.
[236] A. Krishna, S. Gottis, M. K. Nazeeruddin, F. Sauvage, *Adv. Funct. Mater.* **2019**, *29*, 1806482.
[237] L. Chao, T. Niu, Y. Xia, X. Ran, Y. Chen, W. Huang, *J. Phys. Chem. Lett.* **2019**, *10*, 1173.
[238] A. a. O. El-Ballouli, O. M. Bakr, O. F. Mohammed, *J. Phys. Chem. Lett.* **2020**, *11*, 5705.
[239] H. Dong, J. Sun, S. Ma, J. Liang, T. Lu, Z. Jia, X. Liu, B. Xu, *Phys. Chem. Chem. Phys.* **2016**, *18*, 6901.
[240] I. Sayed, S. Bedair, *IEEE J. Photovoltaics* **2019**, *9*, 402.
[241] X. Zhu, Z. Xu, S. Zuo, J. Feng, Z. Wang, X. Zhang, K. Zhao, J. Zhang, H. Liu, S. Priya, *Energy Environ. Sci.* **2018**, *11*, 3349.
[242] Y. Gao, E. Shi, S. Deng, S. B. Shiring, J. M. Snaider, C. Liang, B. Yuan, R. Song, S. M. Janke, A. Liebman-Peláez, *Nat. Chem.* **2019**, *11*, 1151.
[243] A. Stuchebrukhov, *Laser Phys.* **2010**, *20*, 125.
[244] M. Vinoslavskii, P. Belevskii, V. Poroshin, V. Vainberg, N. Baidus, *Low Temp. Phys.* **2020**, *46*, 633.
[245] M. Yu, C. Yi, N. Wang, L. Zhang, R. Zou, Y. Tong, H. Chen, Y. Cao, Y. He, Y. Wang, *Adv. Opt. Mater.* **2019**, *7*, 1801575.
[246] L. Mao, W. Ke, L. Pedesseau, Y. Wu, C. Katan, J. Even, M. R. Wasielewski, C. C. Stoumpos, M. G. Kanatzidis, *JACS* **2018**, *140*, 3775.
[247] B.-E. Cohen, Y. Li, Q. Meng, L. Etgar, *Nano Lett.* **2019**, *19*, 2588.
[248] Y. Li, J. V. Milić, A. Ummadisingu, J.-Y. Seo, J.-H. Im, H.-S. Kim, Y. Liu, M. I. Dar, S. M. Zakeeruddin, P. Wang, *Nano Lett.* **2018**, *19*, 150.
[249] D. Lu, G. Lv, Z. Xu, Y. Dong, X. Ji, Y. Liu, *J. Am. Chem. Soc.* **2020**, *142*, 11114.
[250] B. Bernardo, D. Cheyns, B. Verreet, R. Schaller, B. P. Rand, N. Giebink, *Nat. Commun.* **2014**, *5*, 3245.
[251] L. Mao, H. Tsai, W. Nie, L. Ma, J. Im, C. C. Stoumpos, C. D. Malliakas, F. Hao, M. R. Wasielewski, A. D. Mohite, *Chem. Mater.* **2016**, *28*, 7781.
[252] N. R. Venkatesan, A. Mahdi, B. Barraza, G. Wu, M. L. Chabinyc, R. Seshadri, *Dalton Trans.* **2019**, *48*, 14019.
[253] S. Deng, J. M. Snaider, Y. Gao, E. Shi, L. Jin, R. D. Schaller, L. Dou, L. Huang, *J. Chem. Phys.* **2020**, *152*, 044711.
[254] M. Braun, W. Tuffentsammer, H. Wachtel, H. Wolf, *Chem. Phys. Lett.* **1999**, *307*, 373.
[255] J. Leveillee, C. Katan, J. Even, D. Ghosh, W. Nie, A. D. Mohite, S. Tretiak, A. Schleife, A. J. Neukirch, *Nano Lett.* **2019**, *19*, 8732.
[256] D. B. Mitzi, K. Chondroudis, C. R. Kagan, *Inorg. Chem.* **1999**, *38*, 6246.
[257] Y. Gao, Z. Wei, P. Yoo, E. Shi, M. Zeller, C. Zhu, P. Liao, L. Dou, *JACS* **2019**, *141*, 15577.
[258] N. A. Minder, S. Ono, Z. Chen, A. Facchetti, A. F. Morpurgo, *Adv. Mater.* **2012**, *24*, 503.
[259] V. C. Sundar, J. Zaumseil, V. Podzorov, E. Menard, R. L. Willett, T. Someya, M. E. Gershenson, J. A. Rogers, *Science* **2004**, *303*, 1644.
[260] K. Kikuchi, Y. Takeoka, M. Rikukawa, K. Sanui, *Curr. Appl. Phys.* **2004**, *4*, 599.
[261] D. B. Mitzi, C. D. Dimitrakopoulos, L. L. Kosbar, *Chem. Mater.* **2001**, *13*, 3728.
[262] H. Němec, I. Kratochvilova, P. Kužel, J. Šebera, A. Kochalska, J. Nožár, S. Nešpůrek, *Phys. Chem. Chem. Phys.* **2011**, *13*, 2850.
[263] S. R. Walter, J. Youn, J. D. Emery, S. Kewalramani, J. W. Hennek, M. J. Bedzyk, A. Facchetti, T. J. Marks, F. M. Geiger, *JACS* **2012**, *134*, 11726.

Dumitru Sirbu received his Ph.D. in 2015 at the Institute of Chemistry of ASM, within the Marie Curie IRSES Moldova-Romania-UK framework. He then pursued postdoctoral research in the Molecular Photonics Laboratory at Newcastle University, UK. In 2018, he joined the Perovskite Laboratory in the Emerging Technologies & Materials group and since 2020 is a Postdoctoral Fellow in the Photonics Group at the School of Mathematics, Statistics, and Physics. Currently, his research focuses on metal-free and layered perovskite materials for nonlinear photonics and photovoltaic applications.

Folusho Helen Balogun is a Ph.D. student studying physics at the University of Warwick. She received her integrated master's degree from Queen Mary University. Her research focus is on analyzing halide perovskite materials using terahertz spectroscopy, transient absorption spectroscopy, and time-correlated single-photon counting.

Rebecca L. Milot is currently an Assistant Professor in the Department of Physics at the University of Warwick. She received her Ph.D. in Chemistry from Yale University in 2014 under the direction of Charles Schmuttenmaer and was a postdoctoral research assistant at the University of Oxford from 2014 to 2018 in the groups of Michael Johnston and Laura Herz. Her research focuses on studying the optoelectronic properties of materials with solar energy applications, including metal halide perovskites, using THz spectroscopy and other ultrafast spectroscopic techniques.

Pablo Docampo received his DPhil in 2012 from the University of Oxford focussing on solid-state dye-sensitized solar cells. He became interested in hybrid perovskites which he further developed in his postdoctoral research stay with Thomas Bein at the LMU Munich in 2013. There, he was appointed assistant professor and Marie Curie Fellow between 2014 and 2016 and obtained his 'habilitation' in Physical Chemistry. Dr. Docampo has led a research group investigating the long-term applications of perovskite materials, from the development of new materials and solar cell device architectures to new lighting applications such as lasers, LEDs and LECs.